*Appendix C*

# Reprints of Published Articles

Neuron, Vol. 30, 489–502, May, 2001, Copyright ©2001 by Cell Press

# Dynamic Visualization of Local Protein Synthesis in Hippocampal Neurons

**Girish Aakalu,[2] W. Bryan Smith,[2] Nhien Nguyen, Changan Jiang, and Erin M. Schuman[1]**
Caltech
Howard Hughes Medical Institute
Division of Biology 216-76
Pasadena, California 91125

## Summary

**Using pharmacological approaches, several recent studies suggest that local protein synthesis is required for synaptic plasticity. Convincing demonstrations of bona fide dendritic protein synthesis in mammalian neurons are rare, however. We developed a protein synthesis reporter in which the coding sequence of green fluorescent protein is flanked by the 5′ and 3′ untranslated regions from CAMKII-α, conferring both dendritic mRNA localization and translational regulation. In cultured hippocampal neurons, we show that BDNF, a growth factor involved in synaptic plasticity, stimulates protein synthesis of the reporter in intact, mechanically, or "optically" isolated dendrites. The stimulation of protein synthesis is blocked by anisomycin and not observed in untreated neurons. In addition, dendrites appear to possess translational hot spots, regions near synapses where protein synthesis consistently occurs over time.**

## Introduction

The discovery that polyribosomes are located near the base of many spines (Steward and Levy, 1982) in the hippocampus suggested the possibility that neuronal proteins can be synthesized in dendrites. In theory, the synthesis of proteins in dendrites provides a mechanism by which synapses can independently control their strength, circumventing the need for precisely addressed protein transport from the soma (Schuman, 1999a). In the context of synaptic plasticity, then, the ability to locally synthesize proteins allows synapses to solve the problem of maintaining "specificity" *and* obtaining the newly synthesized proteins required for long-term synaptic plasticity (Frey et al., 1988; Kang et al., 1997; Nguyen et al., 1994; Otani et al., 1989; Stanton and Sarvey, 1984).

In the past 5 years, several studies have shown that locally synthesized proteins likely contribute to long-lasting synaptic plasticity (reviewed in Schuman, 1999a; Steward and Schuman, 2001; Wells et al., 2000). In hippocampal slices, BDNF-induced synaptic plasticity is blocked by inhibitors of protein synthesis (Kang and Schuman, 1996). In the same study, Schaffer-collateral CA1 synapses that were isolated from their pre- and postsynaptic cell bodies still exhibited protein synthesis-dependent plasticity, suggesting a local, dendritic source of protein synthesis. A similar dependence on dendritic protein synthesis has been observed for metabotropic receptor-induced LTD at Schaffer-collateral CA1 synapses in the hippocampus (Huber et al., 2000). Long-term facilitation induced by 5-HT at cultured sensory motoneuron synapses in *Aplysia* also shows a requirement for local protein synthesis in the sensory neuron (Casadio et al., 1999; Martin et al., 1997). In addition, 5-HT application to isolated sensory neurites results in new protein synthesis (Martin et al., 1997). Most demonstrations of dendritic protein synthesis have relied on biochemical fractionation techniques to isolate fragments of dendrites and postsynaptic spines (e.g., the synaptoneurosome). In these studies, the incorporation of radiolabeled amino acids into new proteins demonstrated that synthesis can clearly occur in these dendritically derived fractions (Rao and Steward, 1991; Weiler and Greenough, 1991, 1993). The use of a cell culture system in which the cell bodies are separated from the dendrites also showed that isolated dendrites can synthesize proteins (Torre and Steward, 1992) and glycosylate proteins (Torre and Steward, 1996). The drawbacks of the above techniques include the possibility of contamination by nondendritic fractions, the removal from a physiological context, and the lack of temporal resolution. Here we describe the development of a high-fidelity dendritic protein synthesis reporter and show unequivocally that protein synthesis can be stimulated in dendrites by BDNF, a growth factor involved in synaptic plasticity.

## Results

### BDNF Stimulates Protein Synthesis of a GFP Reporter in Hippocampal Neurons

In order to examine dendritic protein synthesis dynamically in living neurons, we constructed a green fluorescent protein (GFP) reporter, flanked by the 5′ and 3′ untranslated regions (UTR) from the $Ca^{2+}$/calmodulin-dependent kinase II-α subunit (CAMKII-α) (5′GFP3′). Previous work has shown that the 3′UTR of the CAMKII-α mRNA contains information sufficient for its dendritic localization (Mayford et al., 1996; Mori et al., 2000). In initial experiments, the 5′GFP3′ reporter was introduced into cultured neurons using Biolistics. In expressing neurons, GFP was present in the soma and the dendrites, as indicated by immunolabeling for the dendritic marker MAP2 (Figure 1A). In most untreated neurons, expression of the reporter was robust in the cell bodies and relatively weak in the associated dendritic processes (Figure 1B). We examined whether exposure to BDNF modified the levels and/or pattern of GFP expression in neurons; 6 hr after transfection, dishes were exposed to either BDNF (50 ng/ml) or a control (HBS) solution for 4 hr. Neurons that were exposed to BDNF exhibited an increase in GFP synthesis that was evident in both the cell body and the dendrites (Figure 1B). The analysis of total fluorescence in the dendrites revealed that BDNF-treated neurons had significantly greater quantities of

[1] Correspondence: schumane@its.caltech.edu
[2] These authors contributed equally to this work.

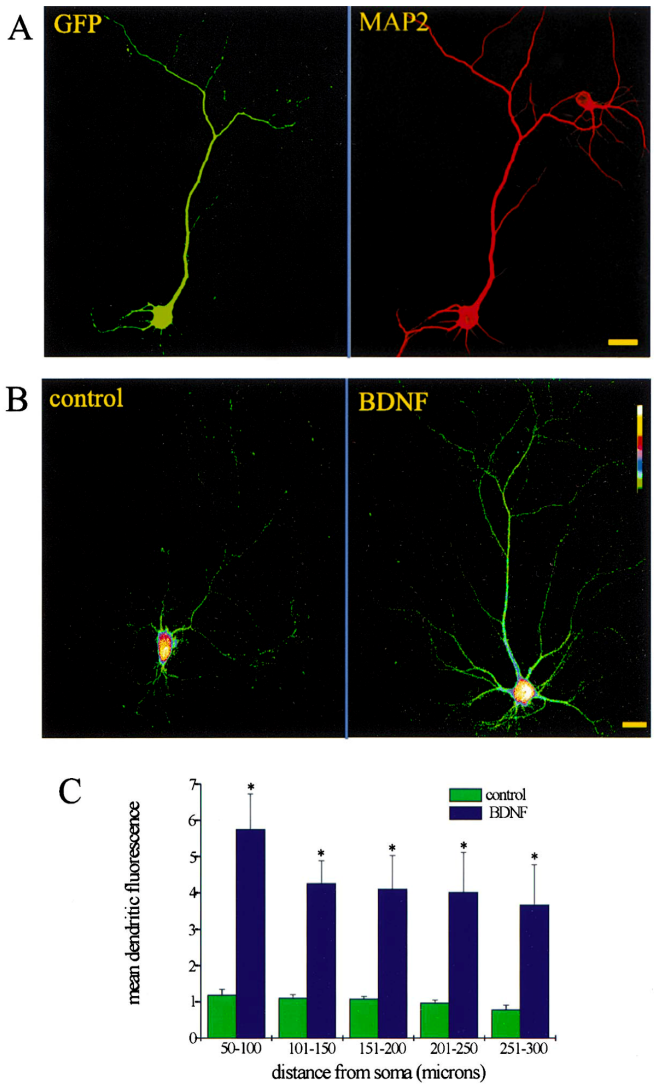


Figure 1. BDNF Stimulates Protein Synthesis of the GFP Reporter in Hippocampal Neurons

(A) Shown is a cultured hippocampal neuron expressing the GFP reporter and immunostained for the dendritic marker MAP2. The majority of the GFP signal occurs in the dendrites, as indicated by the coincident MAP2 signal. Scale bar = 15 μm.

(B) Shown are an untreated and BDNF-treated neuron expressing the GFP reporter. The BDNF-treated cell shows enhanced fluorescence in the cell body and dendrites when compared to the untreated cell. Color lookup bar shows that the absence of GFP signal is indicated by black, increasing fluorescence is indicated by transitions to green, blue, red, and yellow, and saturated fluorescence is indicated by white. Scale bar = 15 μm.

(C) Summary data for all untreated (n = 7) and BDNF-treated (n = 10) dendrites. BDNF-treated neurons showed significantly greater fluorescence ($p < 0.01$) in all dendritic compartments (e.g., 50–300 μm from the soma).

GFP throughout the length of the dendritic process (Figure 1C). These experiments demonstrate that BDNF can stimulate protein synthesis in hippocampal neurons but do not indicate the cellular compartment (e.g., dendrites and/or soma) where the synthesis is occurring.

**Time-Lapse Imaging of BDNF-Stimulated Translation**

In an effort to ascertain the source of the increased GFP synthesis apparent in the above experiments, we conducted time-lapse imaging. We monitored the localization and levels of the GFP reporter over time in individual neurons before and after BDNF treatment. To facilitate the expression of the reporter in a larger population of neurons, we incorporated the reporter construct into a Sindbis virus system (see Experimental Procedures). (We used a destabilized version of GFP, dGFP, in order to decrease the cumulative fluorescence that ultimately contributes to signal saturation.) Dishes of cultured hippocampal neurons were infected with Sin-5′dGFP3′; initial images were collected 12 hr after infection, at a time when the fluorescence had reached steady-state levels. Untreated neurons, imaged over a 4 hr period, showed stable or declining fluorescence in the dendrites and cell body over time (Figures 2A and 2B). In contrast, neurons that were treated with BDNF showed increases in GFP fluorescence that were evident within 60 min of BDNF addition (Figures 2A and 2B). BDNF-induced increases in fluorescence were apparent in both the dendritic and somatic compartments. Of particular interest was the observation of increases in fluorescence in remote aspects of the dendrites (see boxed regions in Figure 2A); these increases were detected as early as

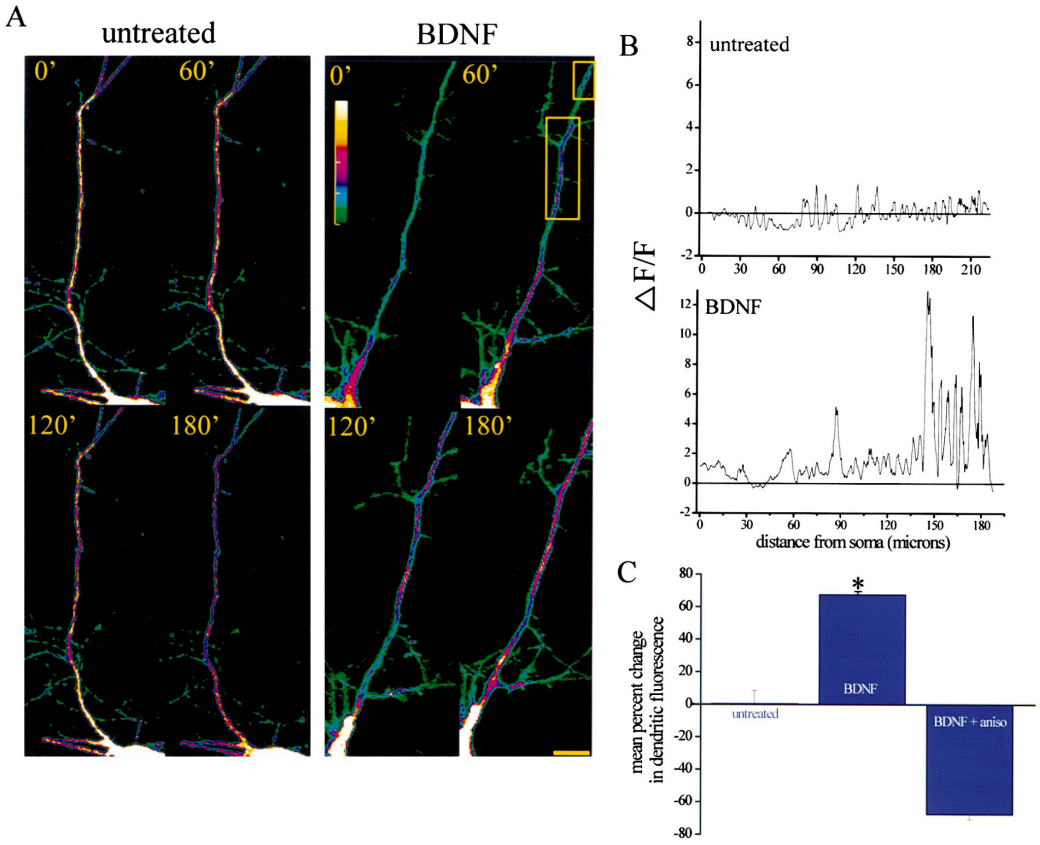


Figure 2. Time-Lapse Imaging of BDNF-Stimulated Translation

(A) Repeated images of a control neuron and BDNF-treated neuron. BDNF was added immediately after the 0 min image was acquired. The BDNF-treated neuron showed increased fluorescence in the dendrite whereas the control neuron was relatively stable over time. Scale bar = 15 μm.

(B) Analysis of the individual neurons shown in (A). ΔF/F was calculated using the data from the 0 and 120 min images (see Experimental Procedures).

(C) Summary data for analysis of total dendritic length showing that only dendrites treated with BDNF exhibited significant ($p < 0.01$) increases in fluorescence.

the increases observed in the cell body, consistent with the notion that GFP is synthesized locally. Overall, when the total length of the dendrite was analyzed, we found that only BDNF-treated neurons showed significant increases in dendritic GFP fluorescence; the average increase in fluorescence was roughly 60%. This is likely a very conservative estimate of BDNF's actions since the analysis includes both synaptic and nonsynaptic areas of the dendrite. For example, our analysis of changes at individual "hot spots," which may correspond to synaptic sites (see below), indicates that BDNF-induced increases in GFP fluorescence ranged from ~1- to 8-fold. Untreated neurons showed no significant increase in dendritic fluorescence when examined over the same time periods (Figure 2C). In addition, the BDNF-induced increases were prevented by coapplication of the protein synthesis inhibitor anisomycin (Figure 2C). In BDNF-treated neurons, we also observed, however, what appeared to be the diffusion of GFP from the soma into the dendrite. This observation prevented us from concluding, unambiguously, that all of the increases in dendritic GFP we observed were due to local synthesis.

### BDNF Stimulates Protein Synthesis in Healthy, Mechanically Isolated Dendrites

In order to remove the cell body as a potential source of GFP signal, we performed dendritic transections in which the dendrites were physically isolated from the cell bodies using a micropipette. Ensuring neuron health and viability following such transections was a major concern. Of approximately 300 transections performed over a 2 year period, only 10 transected neurons fulfilled the health and viability criteria we established for use in experiments (see Experimental Procedures). Technical difficulty aside, the transected dendrite can provide the

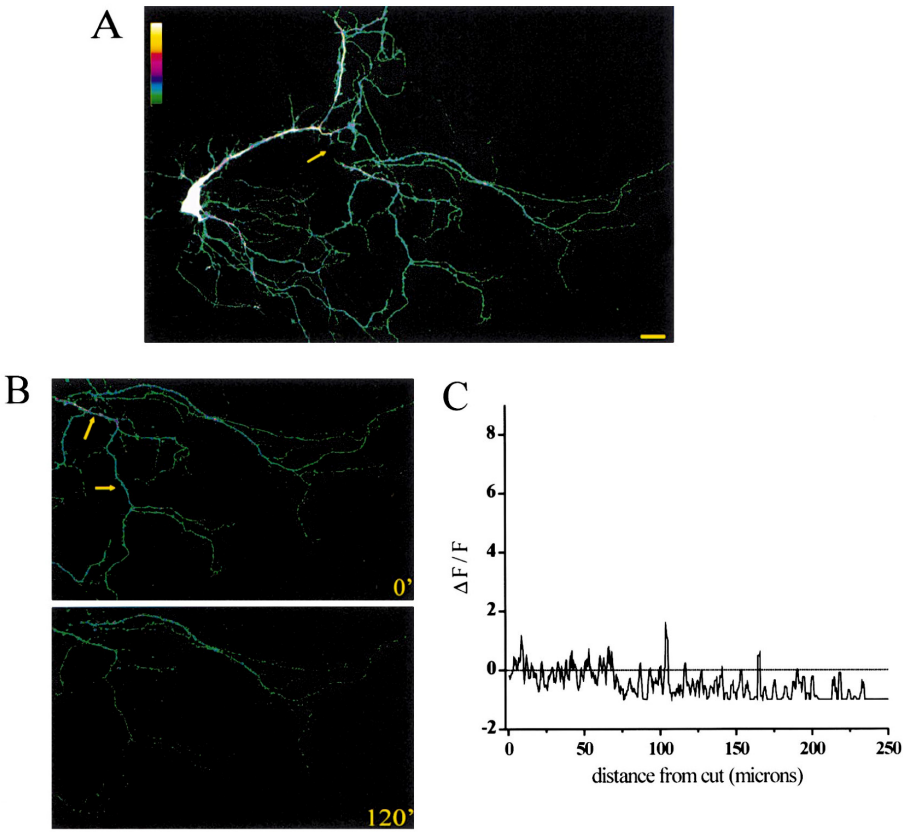


Figure 3. Untreated, Transected Dendrites Do Not Show Increases in Protein Synthesis

(A) Image of an infected neuron; arrow points to the region of transection. Scale bar = 15 μm.

(B) Images of the isolated region of the dendrite immediately following transection and 120 min later. The fluorescent signal in the dendrite decreases over time. Arrows point to the dendrite chosen for analysis in (C). The top dendrite was also analyzed and included in the group analysis (Figure 5).

(C) Analysis of the transected dendrite shown in (A) and (B). ΔF/F was calculated using the data from the 0 and 120 min images (see Experimental Procedures).

most unambiguous proof of local protein synthesis. As before, neurons were infected with Sin-5′dGFP3′. Transected dendrites that were not treated with BDNF usually showed declining fluorescence when monitored over time (Figure 3). In contrast, transected dendrites treated with BDNF exhibited increases in fluorescence in the isolated dendrites (Figure 4). As would be expected, BDNF-induced increases in fluorescence were also observed in the soma and the intact dendrites. The BDNF-induced increases in GFP fluorescence observed in the dendrites were blocked by cotreatment with anisomycin, indicating that the enhanced fluorescence was due to new protein synthesis (Figure 5). Plotting the distribution of changes in pixel intensity over time demonstrated that most regions of transected dendrites treated with BDNF showed increases in intensity (Figure 5C). In contrast, most regions of untreated dendrites or those treated with anisomycin plus BDNF tended to decrease in intensity. (Note that the small number of pixels that increased in intensity in the presence of anisomycin must represent the redistribution of pixels from adjacent areas of the dendrite or the contribution of synthesized, but not yet fluorescent GFP [e.g., Cubitt et al., 1995].) Taken together, these data clearly show that BDNF can stimulate protein synthesis in isolated dendrites. The local dendritic protein synthesis we observed was robust and stable over time.

### A Membrane-Anchored GFP Reporter Exhibits Extremely Limited Diffusion

Because of technical difficulty and the potential for compromising long-term neuronal health, the transection experiments are not a viable option for extensive explorations of local protein synthesis. We reasoned that modifications to the protein synthesis reporter that limited its diffusion would also decrease the potential contribution of somatically synthesized GFP to the signal observed in dendrites. Toward this end, we conferred membrane localization to the reporter by adding a myristoylation consensus sequence (Patrick et al., 1999) at

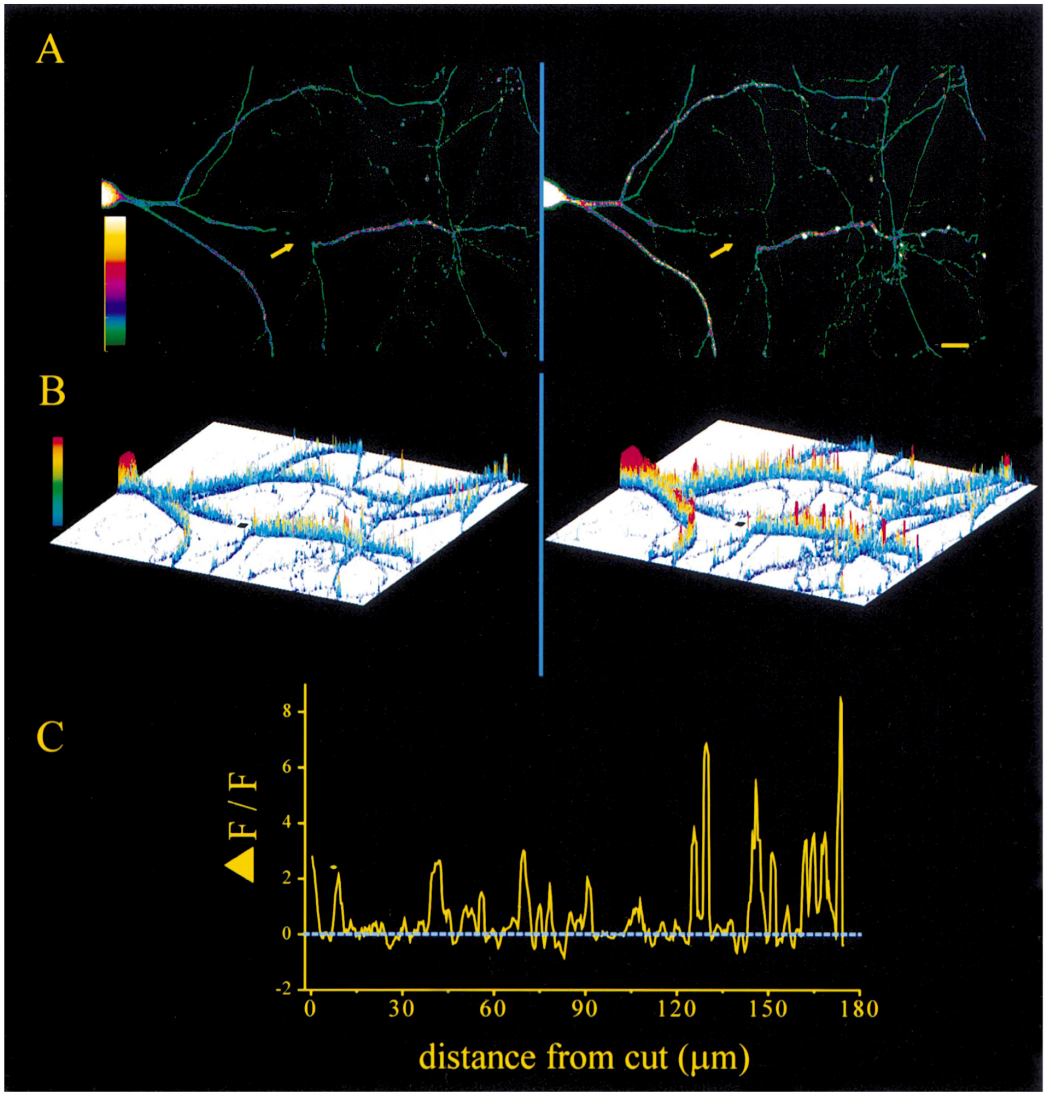


Figure 4. BDNF Stimulates Protein Synthesis in Healthy, Mechanically Isolated Dendrites

(A) Images of transected neuron before (left) and 120 min after (right) BDNF treatment; arrow points to the region of transection. The fluorescent signal in the transected dendrite increases following BDNF treatment. Scale bar = 15 μm.

(B) X-Y-Z plot of the neuron shown in (A) in which changes in fluorescence are indicated by both changes in color and changes in the height of the pixels shown.

(C) Analysis of the transected dendrite shown in (A) and (B). ΔF/F was calculated using the data from the 0 and 120 min images (see Experimental Procedures).

the N terminus of the GFP molecule and expressed this construct, Sin-5′$_{myr}$dGFP3′, in neurons using Sindbis virus. We compared the diffusion of Sin-5′dGFP3′ and Sin-5′$_{myr}$ dGFP3′ by conducting FRAP (fluorescence recovery after photobleaching) experiments in dendrites. Note that the recovery of reporter fluorescence in dendrites following photobleaching is due to both diffusion from the adjacent (nonbleached) compartment as well as new synthesis of the reporter in the bleached domain. To monitor the contribution of diffusion exclusively, we included anisomycin in the bath. In the nonmembrane anchored version of the reporter (Sin-5′dGFP3′), there was substantial recovery of fluorescence in the bleached dendrite within 60 min (Figure 6A). We found that the addition of the myr sequence, however, severely retarded the diffusion of the modified (Sin-5′$_{myr}$dGFP3′)

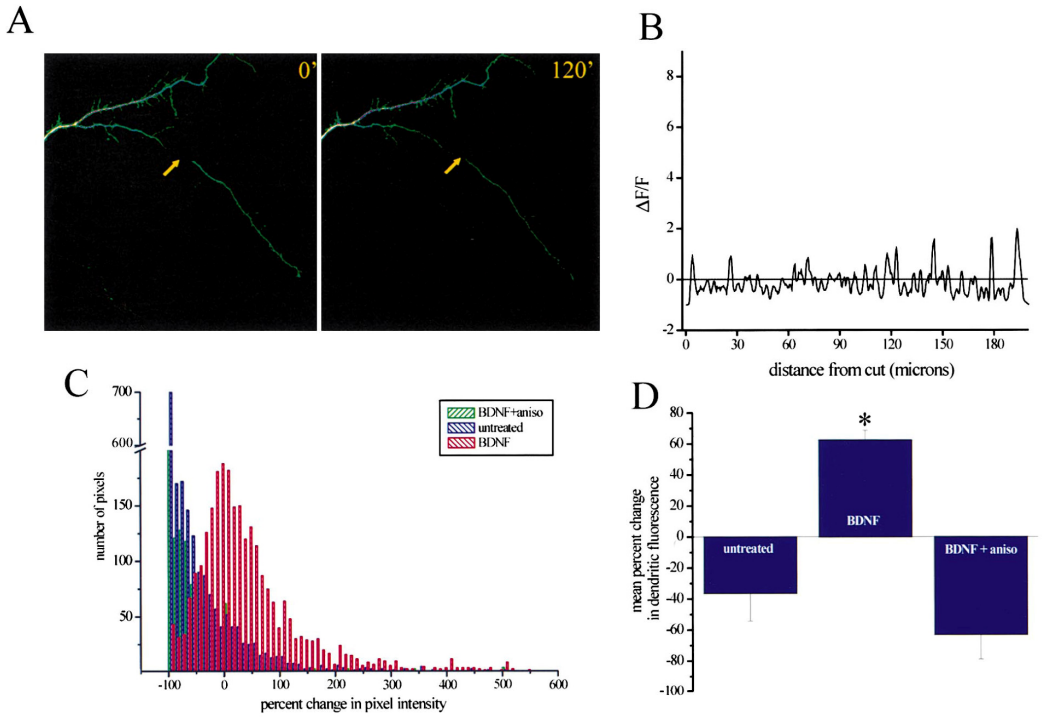


Figure 5. Anisomycin Prevents BDNF-Induced Increases in Protein Synthesis in Transected Dendrites

(A) Images of a transected dendrite before and 120 min after coapplication of BDNF and anisomycin; arrow points to the region of transection. The fluorescent signal in the transected dendrite decreased over time. Arrows indicate the site of transection. Scale bar = 15 μm.

(B) Analysis of the transected dendrite shown in (A). ΔF/F was calculated using the data from the 0 and 120 min images (see Experimental Procedures).

(C) Summary histogram indicating the pixel intensity distributions for all untreated, BDNF-treated, and BDNF plus anisomycin-treated transected dendrites.

(D) Summary diagram indicating the mean percent change in pixel intensity for the three groups. Only the BDNF-treated dendrites showed a signficant increase in fluorescence intensity over time ($p \leq 0.01$). N (cells, dendrites) for each group are as follows: untreated (3, 4); BDNF (4, 5); BDNF + aniso (3, 4).

reporter (Figure 6A). Negligible recovery from the photobleached state was observed in the 120 min following the photobleaching episode. These data indicate that the myristoylated reporter exhibits limited diffusion (see Experimental Procedures), suggesting that it can be used to faithfully report local protein synthesis in intact dendrites.

### BDNF Stimulates Protein Synthesis in Healthy, "Optically Isolated" Dendrites

We next used the diffusion-restricted reporter (Sin-5′$_{myr}$dGFP3′) in combination with photobleaching to examine dendritic protein synthesis in intact neurons. In these experiments, we continuously photobleached the cell body in order to abolish the contribution of somatically synthesized GFP to the dendritic signal; in this way we "optically isolated" the dendrites of interest. The continuous photobleaching of the soma did not compromise neuronal health: propidium iodide labeling of bleached cells revealed no incorporation of the dye (see Experimental Procedures). When we analyzed untreated, optically isolated dendrites, we found that the fluorescence of the reporter decreased over time at most dendritic sites (Figures 6B and 6C). We occasionally observed small (e.g., 0- to 5-fold) fluorescence increases at some sites. These small increases in signal reflect either the redistribution of GFP from adjacent dendritic sites or bona fide new protein synthesis. The

Figure 6. A Membrane-Anchored GFP Reporter Exhibits Limited Diffusion

(A) Shown are two neurons infected with either 5′dGFP3′ or the membrane-anchored 5′$_{myr}$dGFP3′. Neurons were treated with anisomycin for 1 hr prior to the initiation of photobleaching (boxed region shows bleached area). FRAP was monitored in each neuron over time. The neuron infected with the diffusible reporter (5′dGFP3′) showed significant recovery of fluorescence within 60 min of the photobleaching. In contrast, the myristoylated reporter showed negligible recovery within 2 hr following photobleaching. Scale bars: 5′dGFP3′, 15 μm; 5′$_{myr}$dGFP3′, 10 μm.

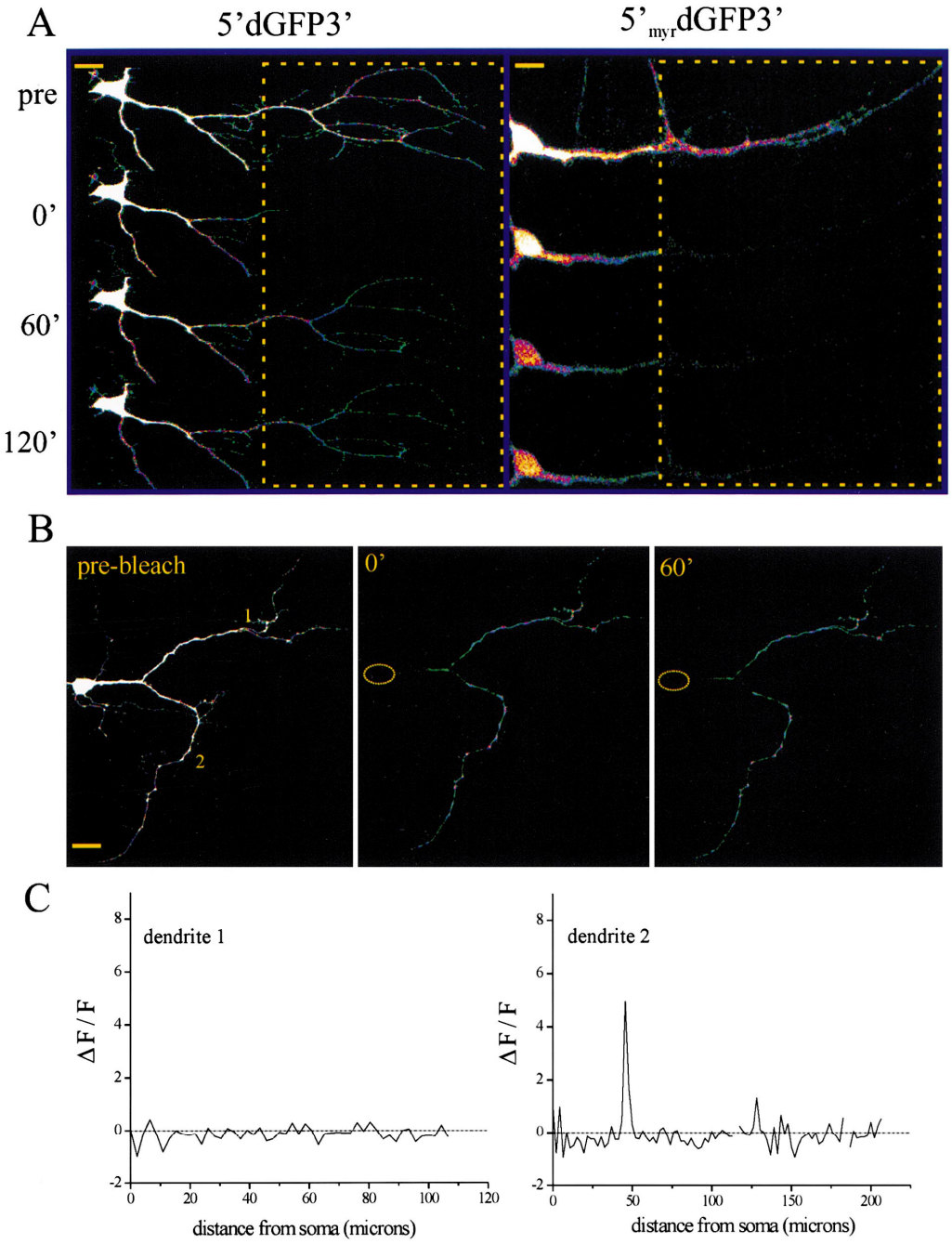


(B) Time-lapse images of a 5′$_{myr}$dGFP3′-expressing neuron that was subjected to somatic photobleaching for the duration of the experiment. The prebleached neuron is shown at the right and two consecutive time points following photobleaching are shown in the middle and left. In this untreated neuron there was an overall decline in dendritic fluorescence during the experiment. Scale bar = 15 μm.
(C) Profile of fluorescence changes between 0 and 60 min for dendrites 1 and 2 (labeled in [B]). In the profiles shown, the mean change in fluorescence between t = 0 and t = 60 was −15.4% and −12.3% for dendrite 1 and 2, respectively.

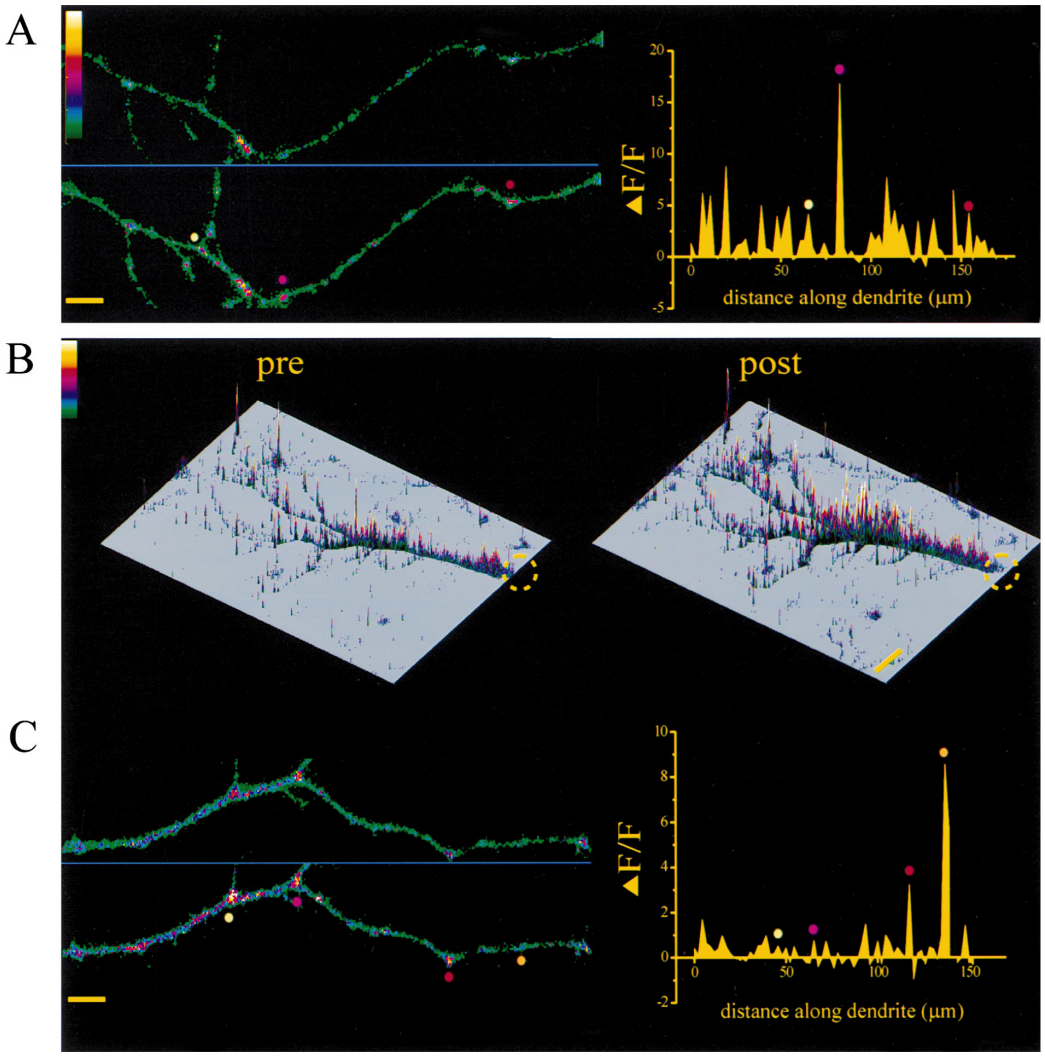


Figure 7. BDNF Stimulates Protein Synthesis in Healthy, "Optically Isolated" Dendrites

(A) Shown is BDNF-induced enhancement of GFP translation in an optically isolated dendrite at two consecutive time points. The profile of fluorescence change between the two time points shown is plotted on the right. Individual hot spots are identified by colored circles on the image and the corresponding profile. Scale bar = 5 μm.

(B) An X-Y-Z plot of a different neuron in which the dendrites were optically isolated. The region of the bleached soma is shown by the dashed circle. The effects of BDNF are evident in comparing the dendritic fluorescence in the pre and post images. Scale bar = 15 μm.

(C) An isolated dendritic segment from the neuron shown in (B) at two different time points. The profile of fluorescence change between the two time points shown is plotted on the right. Individual hot spots are identified by colored circles on the image and the corresponding profile. Scale bar = 5 μm.

fact that both untreated and anisomycin-treated dendrites showed similar average fluorescence change profiles (Figure 8) suggests that most of these small increases reflect redistribution from adjacent portions of the dendrite.

In contrast to untreated neurons, the addition of BDNF to optically isolated dendrites resulted in a robust stimulation of protein synthesis. As shown in Figure 7, increases in reporter translation ranging from 1- to 17-fold were observed at many sites along optically isolated dendrites. Sites of decreased fluorescence were not common in BDNF-treated dendrites. The coapplication of anisomycin completely prevented the BDNF-induced increases in GFP fluorescence, confirming that the observed effects of BDNF were due to new protein synthesis (Figure 8). Dendrites that were treated with aniso-

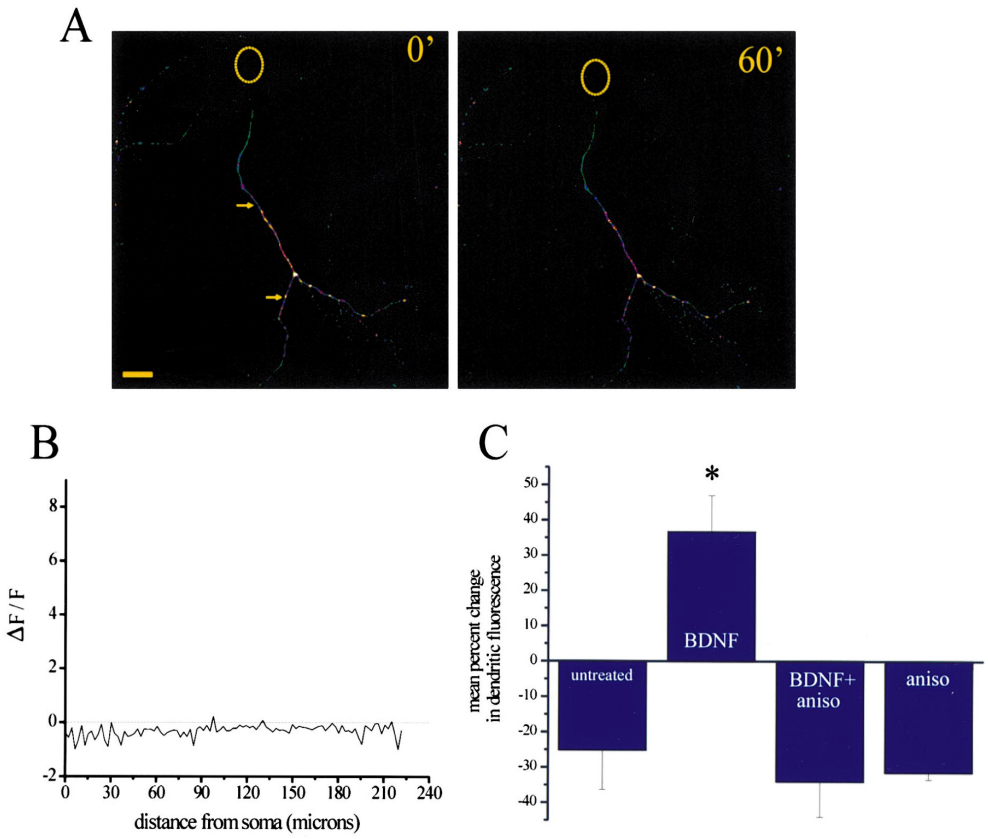


Figure 8. Anisomycin Blocks BDNF-Induced Increases in Protein Synthesis in Optically Isolated Dendrites

(A) Time-lapse images of an optically isolated dendrite that was treated with BDNF plus anisomycin. The optically isolated dendrites are shown at two consecutive time points. There was an overall decline in dendritic fluorescence during the experiment. The area occupied by the photobleached soma is shown by the yellow circle. Scale bar = 15 μm.

(B) Profile of fluorescence changes between 0 and 60 min for dendrite indicated by the arrow in (A). The mean change in fluorescence between t = 0 and t = 60 was −25.7%.

(C) Summary diagram indicating the mean percent change in pixel intensity for all untreated, BDNF-, and BDNF plus anisomycin-, and anisomycin-treated optically isolated dendrites. Only the BDNF-treated dendrites showed a signficant increase in fluorescence intensity over time ($p \leq 0.01$). N (cells, dendrites) for each group are as follows: untreated (4, 6); BDNF (5, 8); BDNF + aniso (4, 5); aniso (3, 5).

mycin alone or anisomycin plus BDNF usually showed decreases in fluorescence along the length of the dendrite interspersed with very small increases that likely represented redistribution of GFP molecules from adjacent regions of the dendrites (Figure 8).

### The Protein Synthesis Reporter Is Concentrated near Sites of Translation and Synapses

Repeated imaging of optically isolated dendrites allowed us to examine the location of GFP signals over time. When the fluorescence intensity profiles derived from time-lapse imaging of an individual dendrite were plotted together, it became clear that the GFP signals appeared to be spatially concentrated at hot spots that were stationary over time (Figure 9). The increases and occasional decreases in GFP signal that were observed over time tended to appear at the same locations along the dendrite. We next examined whether these reporter hot spots were in the vicinity of synaptic sites and/or sites of protein translation. We immunolabeled $5'_{myr}$dGFP3′-expressing cells with an antibody to the postsynaptic marker PSD-95, the presynaptic marker synapsin I, or rRNA (Y10B; Koenig et al., 2000; Lerner et al., 1981). We found that the GFP hot spots often were near ribosomes or synaptic regions as indicated by the proximity of the PSD-95, synapsin, or Y10B signal to GFP (Figure 10). The colabeling for PSD-95 also revealed that the myristoylated reporter appeared not to enter synaptic spines to an appreciable extent and appeared more concentrated in dendritic shafts. As such, we did not expect to observe strict "colocalization" of the GFP signal with the synaptic markers. We did observe, however, that GFP was, much more often than not, in the vicinity of ribosomes and synapses. To quan-

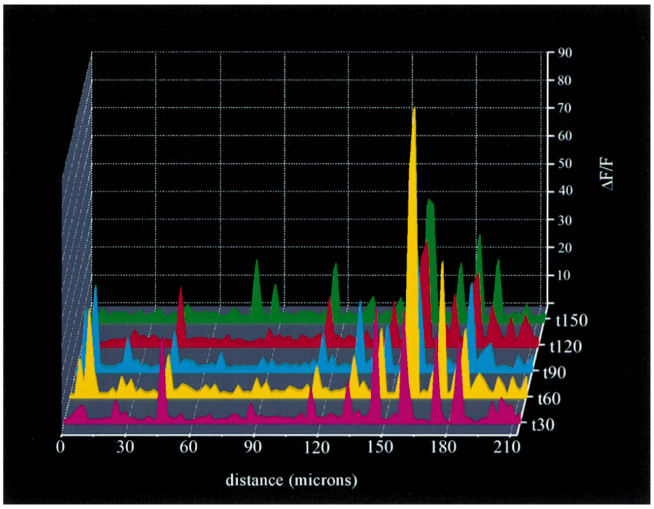


Figure 9. GFP Reporter Signals Are Spatially and Temporally Persistent

Shown are the ΔF/F profiles for a single optically isolated dendrite at several time points. The increased GFP signal is concentrated at relatively stable sites along the length of the dendrites. These sites also appear to be temporally stable over a 2 hr time period.

tify this relationship, we calculated the mean fluorescence for each signal across the dendritic width (thus obtaining mean fluorescence values for the entire length of each dendrite), and calculated the pairwise cross-correlation of GFP and PSD-95, synapsin, or Y10B. A cross-correlation measures the spatial coincidence of the two signals, with the lag value representing the distance one signal must be shifted in order to spatially correlate with the other signal. Analysis of the GFP/Y10B, GFP/synapsin, or GFP/PSD-95 (data not shown) signals revealed a significant cross-correlation between the two signals (Figure 10). The peaks at zero lag for both the GFP/Y10B and GFP/synapsin analysis (Figures 10F and 10G) indicate that the two signals are highly correlated. The observation that locally synthesized GFP is concentrated in the vicinity of ribosomes and synapses suggests that there are local hot spots of translation that are near synaptic sites. These data are predicted to some extent by previous anatomical observations of ribosomes at or near the bases of dendritic spines (Steward and Levy, 1982). The spatially and temporally stable sites of translation that we have identified provide evidence for a central tenet of the local protein synthesis hypothesis—the notion that locally synthesized proteins might be selectively made available to their associated synapses, thus providing a mechanism for synapse specificity (Schuman, 1999a; Steward, 1997; Steward and Schuman, 2001). Whether these observations hold true for other types of locally synthesized proteins (e.g., nonmyristoylated) is an important issue for future studies.

## Discussion

We have described the visualization of dendritic protein synthesis in mature cultured hippocampal neurons. We report a robust stimulation of local protein synthesis by the growth factor BDNF. In the last 5 years, several studies have used clever applications of protein synthesis inhibitors to demonstrate roles for locally synthesized proteins in different forms of synaptic plasticity (Casadio et al., 1999; Huber et al., 2000; Kang and Schuman, 1996; Martin et al., 1997). In *Aplysia* sensory neurons, serotonin application to isolated neurites results in detectable protein synthesis (Casadio et al., 1999). Direct demonstrations of protein synthesis in mature mammalian dendrites are scarce, however. Using radiolabeling, Feig and Lipton (1993) showed that newly synthesized proteins could be detected in dendrites of hippocampal slices—the timing was such that the cell body was unlikely to be the source of protein synthesis. Nevertheless, the difficulty associated with the radiolabeling procedure as well as the troublesome identification of dendritic compartments limits the appeal of this approach. In contrast, the approach we have developed allows the visualization of dendritic protein synthesis in living neurons over time. Ultimately, we combined the use of a membrane-anchored, destabilized GFP with somatic photobleaching to be sure that reporter signals observed in the dendrite were synthesized in the dendrite. Given the limited diffusion of the myristoylated dGFP (e.g., Figure 6), a case could certainly be made for using the myristoylated reporter alone (without somatic photobleaching) in future investigations of dendritic protein synthesis in slice preparations as well as in vivo.

The BDNF-induced increases in GFP fluorescence we observed were completely blocked by anisomycin. Since BDNF does not slow the degradation rate of the GFP reporter (our unpublished data), these data indicate that the fluorescence increases were due to new protein synthesis. In addition, BDNF-induced dendritic protein synthesis was not accompanied by any obvious or systematic changes in cell morphology. We observed increases in GFP reporter within 45–60 min of BDNF application (e.g., Figure 2). Preceding its ability to fluoresce, GFP possesses posttranslational requirements for cyclization and oxidation (Cubitt et al., 1995). As such, GFP is not an optimal reporter for addressing how quickly protein synthesis can occur in dendrites. Previous studies using developing neurons reported that a combination of BDNF and NT-3 (Crino and Eberwine, 1996) or a

metabotropic receptor agonist (Kacharmina et al., 2000) could stimulate translation of a myc epitope in transected growth cones between 1 and 4 hr after transfection. In addition to participating in synaptic plasticity, a role for BDNF-stimulated dendritic protein synthesis might also be imagined in other contexts where BDNF clearly plays an important neurotrophic role in development and the morphology of neurons (McAllister et al., 1999; Schuman, 1999b).

The regulated synthesis of our reporter may mimic the translation of endogenous CAMKII-α since our reporter contains both the 5′ and 3′UTR from the CAMKII-α gene. Indeed, a stimulation of dendritic CAMKII-α translation by LTP has been suggested by immunohistochemical studies (Ouyang et al., 1997, 1999). The 5′UTR may contain translational regulatory elements: we noticed that GFP fluorescence in neurons transfected with a construct lacking the 5′UTR (GFP3′) appeared to be greater than that observed in cells expressing a construct containing both the 5′ and 3′UTR (data not shown). The 3′UTR was included primarily to confer dendritic localization of the GFP mRNA (Mayford et al., 1996; Mori et al., 2000), although this was likely not necessary in the present study given the abundance of the mRNA produced by viral infection. The 3′UTR of CAMKII-α also contains elements for regulation of translation, namely the CPE (cytoplasmic polyadenylation element) and polyadenylation signal (Wu et al., 1998). We have not addressed whether the BDNF-stimulated translation we observe requires these elements, although others have clearly shown regulation of CAMKII-α translation via these and other regulatory elements (Sheetz et al., 2000; Wu et al., 1998).

In addition to its effects on hippocampal slices, BDNF can also facilitate synaptic transmission in cultured hippocampal neurons (Levine et al., 1995; Li et al., 1998a, 1998b). Both pre- and postsynaptic (Levine et al., 1997) mechanisms have been proposed for BDNF's actions on synaptic transmission. In the present experiments, the stimulation of protein synthesis could be due to activation of postsynaptic TrkB receptors and subsequent stimulation of local translation machinery, potentially through the rapamycin-sensitive M-TOR kinase pathway (e.g., Brown and Schreiber, 1996; Casadio et al., 1999; S.J. Tang et al., 1998, Soc. Neurosci., abstract). Alternatively, BDNF could enhance glutamate release from presynaptic terminals (e.g., Li et al., 1998a, 1998b), which could then stimulate postsynaptic protein synthesis through glutamate receptor signaling.

In sum, these data clearly show that dendrites of mammalian neurons can synthesize proteins. The demonstration that dendrites that are in a synaptic network can synthesize proteins provides support for the idea that locally synthesized proteins contribute to synaptic function. The observation that there are spatially and temporally consistent hot spots for translation suggests that local synthesis might play a role in maintaining the specificity of synaptic connections.

## Experimental Procedures

### Cultured Neurons

Dissociated hippocampal neuron cultures are prepared from postnatal 2- and 3-day rat pups as described (Banker and Goslin, 1990). Neurons are plated at a density of 15,000–45,000 cells/cm$^2$ onto poly-l-lysine and laminin-coated coverslips. The cultures are maintained and allowed to mature in growth medium (Neurobasal-A supplemented with B27 and Gluta MAX-1) for 14–21 days before use. In Biolistic experiments, dissociated P2 hippocampal neurons were transfected with the pcDNA3.1-5′GFP3′ construct according to the manufacturer's protocol (Bio-Rad). DNA-gold complexes were generated with the following parameters: 50 μg plasmid DNA, 17 mg 1.6 μm diameter gold particles, and 0.01% PVP. In viral infection experiments, dissociated P2 hippocampal neurons were infected for 12 hr in growth medium containing the Sindbis virus of choice. Six hours post initial transfection or 10–12 hr post initial infection, growth medium was removed and replaced with HEPES-buffered solution (HBS) (Malgaroli and Tsien, 1992) (without glycine or picrotoxin) for imaging. All neurons used in our experiments had a pyramidal neuron-like morphology with one or two major dendrites emanating from the cell body. For immunolabeling, neurons were fixed at room temperature with 4% paraformaldehyde for 20 min. Fixed cultures were then treated sequentially with PBS, PBT (1× PBS, 2 mg/mL BSA, 0.1% Triton X-100), preblock (20% normal goat serum in PBT), primary Ab in preblock at 4°C overnight, preblock, Cy3-conjugated seconday Ab in preblock, preblock, and PBS. Immunostained specimens were imaged in PBS. The sources of the antibodies were as follows: MAP2 (Chemicon), PSD-95 (Upstate Biotechnology), Y10B (generous gift from Jeff Twiss, UCLA), synapsin I (Novus).

### Constructs

pcDNA3.1-5′dGFP3′: The CamKII-α 3′UTR sequence obtained from plasmid (Mayford et al., 1996) was PCR amplified (forward primer: 5′-ttatatttgcggccgcggtcgctaccattaccagtt-3′; reverse primer: 5′-ggc gctctctcgagtttaaatttgtagct-3′) and cloned into the NotI and XhoI sites of the pcDNA3.1 vector (Invitrogen). The resulting vector was then cleaved with BamHI and NotI for insertion of the destabilized EGFP ORF (from pd2EGFP, Clontech). The CamKII-α 5′UTR was released from a plasmid (obtained from J. Fallon) and inserted at the HindIII-BamHI sites, yielding pcDNA-5′dGFP3′. pSinRep5-5′dGFP3′: The 5′dGFP3′ fragment was released with PmeI-ApaI (blunted) and ligated into pSinRep5 (Invitrogen). pcDNA3.1-5′$_{myr}$dGFP3′: The d2EGFP ORF (from pd2EGFP, Clontech) was PCR amplified (forward primer: 5′-cgactctagagtgagcaagggcgaggagctg-3′; reverse primer: 5′-tctagagtcgcggccgcatctacaca-3′), digested, and inserted into the XbaI-NotI sites of pBSK. To generate the myristoylation signal, two oligos corresponding to the N-terminal 10 amino acids of p10 were annealed (myr1: 5′-gatccatgggcacggtgctg tccctgtctcccagct-3′; myr2: 5′-ctagagctgggagacagggacagcaccgtg cccatg-3′), digested, and inserted into the BamHI-XbaI sites of pBSK-d2EGFP. The $_{myr}$dGFP was subcloned into the BamHI-NotI sites of pcDNA3.1-5′dGFP3′. pSinRep5-5′$_{myr}$dGFP3′: The 5′$_{myr}$3 dGFP3′ fragment was released with PmeI-ApaI and subcloned into the StuI-ApaI sites of pSinRep5 (Invitrogen). Sindbis viroids were produced according to the Experimental Procedures provided by Invitrogen. Contrary to observations in other cell types, it appears that single-stranded RNA viruses of the α family do not shut down protein synthesis in neurons (K. Lundstrom, personal communication, Hoffmann-LaRoche, Basel, Switzerland).

### Microscopy

Confocal images were acquired in 0.3 μm sections; image analysis was conducted on z-compressed image stacks that contained the entire neuron of interest. GFP was excited at 488 nm and emitted light was collected between 510–550 nm. Images were acquired with parameters that maximized the dynamic range of pixel intensity for the dendritic signal. Using these parameters, the cell body fluorescence intensity was necessarily, occasionally, saturated. In all experiments, identical acquisition parameters and settings were used for both control and BDNF-treated dendrites on a given experimental day. In time-lapse experiments, the cultured neurons were maintained in an incubator (36.5°C) between image acquisition episodes. Images were acquired at room temperature. The acquisition of images at individual time points took less than 3 min.

### Transections

Cells were preincubated in HBS for 2 hr before the start of transection experiments. Transection was carried out as follows: GFP-

Neuron
500

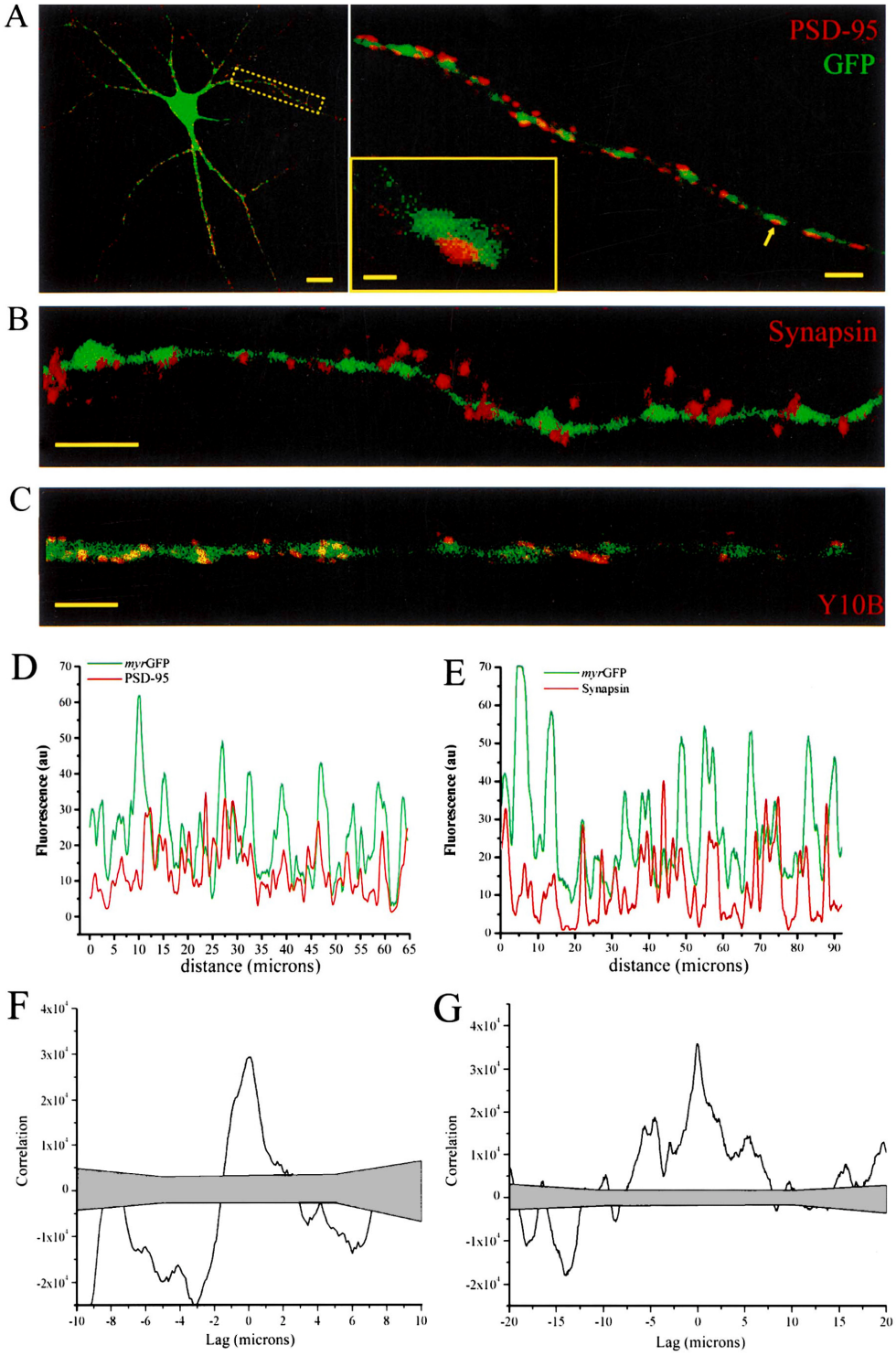
A
PSD-95
GFP
B
Synapsin
C
Y10B
D
myrGFP
PSD-95
Fluorescence (au)
distance (microns)
E
myrGFP
Synapsin
Fluorescence (au)
distance (microns)
F
Correlation
Lag (microns)
G
Correlation
Lag (microns)

expressing neurons were oriented such that the dendritic segment to be cut was in line with the long axis of the microelectrode. The glass microelectrode was then carefully lowered onto the dendrite until a spot of no GFP signal was seen, indicating that the dendrite had been pinched at that point. After allowing the microelectrode to rest in this position for 1-2 min, the electrode was slowly moved down vertically, allowing the tip to flex and push the proximal aspect of the dendrite toward the soma and away from the more distal dendrites. Complete transection of the dendrite as well as the integrity of the dendritic arbor was verified by DIC images. In order to be included in experiments, transected neurons were required to meet the following criteria: (1) both the transected process and the neuron from which it was cut must remain morphologically intact and healthy for the duration of the experiment; (2) no signs of varicosity formation or blebbing; (3) some detectable fluorescence signal must be observed in the transected process 2 hr post transection.

### Photobleaching

In FRAP experiments, an infected neuron was selected and a dendrite from that neuron was scanned for 1 hr with a 488 nm, ~5 mW laser. Complete volumetric data of the dendrite to be studied were acquired at regular intervals before and after the bleaching. In optical isolation experiments, an infected neuron was selected, and its soma was continuously scanned to photobleach the somatic GFP. Propidium iodide (PI) exclusion experiments were conducted to insure neuronal viability during optical isolation experiments. After ~90 min somatic photobleaching, the cell was stained with PI solution (50 μg/ml). The cell was then assessed for PI staining. Positive control experiments utilizing glutamate-induced toxicity (250 μM) were also carried out. No PI staining was evident after somatic photobleaching whereas the glutamate-induced toxicity in the same cells led to strong PI staining. Pilot experiments indicated that complete somatic photobleaching was obtained within 120 min of the initiation of photobleaching. In all experiments, data analysis began with this (complete somatic photobleaching) time point and hence was designated as $t = 0$. Using data from FRAP experiments, we estimate the membrane tethered reporter's diffusion coefficient to be $1 \times 10^{-8}$ cm$^2$/s, which is only slightly greater than the diffusion coefficient of rhodopsin ($\sim 5 \times 10^{-9}$ cm$^2$/s) (Wey et al., 1981) and glycine receptors ($\sim 1 \times 10^{-9}$ cm$^2$/s) (Srinivasan et al., 1990). This difference is expected since rhodopsin and glycine receptors are integral membrane proteins that may be bound to elements in the cytoskeleton and therefore would be more diffusion limited than a myristoylated protein. This estimate of the reporter's diffusion coefficient may include the simultaneous effects of degradation on the reporter. Indeed, there are examples of FRAP experiments where the rate of degradation of the reporter exceeded the rate of diffusion of the reporter.

### Analysis

To analyze the GFP of individual dendrites, we calculated the mean pixel intensity for each dendrite along its length (NIH Image, Scion Image, or Image J), thus controlling for changes in the width of the dendrite. In time-lapse experiments, we calculated a normalized difference score, $\Delta F/F(y - x/x)$, that indicates the change in dendritic fluorescence as a function of time and, when appropriate, treatment with BDNF. In plotting $\Delta F/F$, the data were binned into 1–2 μm sections. In regular time-lapse and dendritic transection experiments, x was the baseline (first) fluorescence measurement and y was the brightest time point following the baseline (typically 120 min). In "optical isolation" experiments, x was chosen as the lowest time point following somatic photobleaching and y was usually taken 60 min later. All untreated cells were "yoked" to experimental cells. That is, they were infected at the same time, imaged at equivalent time points, and the analysis was calculated using the same time points as their BDNF-treated "sister" neurons. For analysis of colocalization, horizontal dendritic segments were analyzed by obtaining the mean fluorescence signal across the width of the dendritic segment. A cross-correlation was calculated for the $_{myr}$dGFP and PSD-95, synapsin, or Y10B: the mean fluorescence across the width of a dendritic segment was calculated, generating a one-dimensional representation of the relative amplitudes of the red and green signals. A cross-correlation was calculated on these two data sets. To calculate the significance of the cross-correlation, one hundred cross-correlations of the randomized data were performed to yield a 95% confidence level. In other experiments, Student's t tests were performed to assess statistical differences between groups. We chose for analysis the brightest (usually principal) dendrite from each neuron in each group. When a single neuron possessed two bright, principal dendrites, both were used in the analysis.

### Acknowledgments

We are grateful to Gilles Laurent and members of the Schuman lab for criticism and discussion. We thank Michael Tsung and Holli Weld for making beautiful cultured neurons. We thank Jeff Twiss for the Y10B antibody. This work was supported by Howard Hughes Medical Institute.

Received February 23, 2001; revised April 17, 2001.

### References

Banker, G., and Goslin, K. (1990). Culturing nerve cells (Cambridge, MA: MIT Press).

Brown, E.J., and Schreiber, S.L. (1996). A signaling pathway to translational control. Cell *86*, 517–520.

Casadio, A., Martin, K.C., Giustetto, M., Zhu, H., Chen, M., Bartsch, D., Bailey, C.H., and Kandel, E.R. (1999). A transient, neuron-wide form of CREB-mediated long-term facilitation can be stablized at specific synapses by local protein synthesis. Cell *99*, 221–237.

Crino, P.B., and Eberwine, J. (1996). Molecular characterization of the dendritic growth cone: regulated mRNA transport and local protein synthesis. Neuron *17*, 1173–1187.

Cubitt, A.B., Heim, R., Adams, S.R., Boyd, A., and Gross, L.A. (1995). Understanding, improving and using green fluorescent proteins. Trends Biochem. Sci. *20*, 448–455.

Feig, S., and Lipton, P. (1993). Pairing the cholinergic agonist carbachol with patterned schaffer collateral stimulation initiates protein

Figure 10. GFP Reporter Signals Colocalize with Ribosomes and Synaptic Markers

(A) Low- (left) and high-power (right) images of a GFP reporter-expressing neuron immunostained with an antibody against the synaptic marker PSD-95. The inset shows the GFP signal that forms a cloud around the punctate PSD-95 signal. Scale bars = 15, 5, and 1 μm, for low-, high-power, and inset images, respectively.

(B) High-power image of a GFP reporter-expressing neuron immunostained with an antibody against the presynaptic protein synapsin I, showing that the GFP signal is often in the vicinity of the presynaptic marker.

(C) High-power image of a GFP reporter-expressing neuron immunostained with an antibody against the ribosomal marker Y10B.

(D) Fluorescence intensity plots for the GFP and PSD-95 signals of the dendrite shown in (A). The mean fluorescence along the width of the dendrite was calculated.

(E) Fluorescence intensity plots for the GFP and synapsin signals of the dendrite shown in (B). The mean fluorescence along the width of the dendrite was calculated.

(F) The cross-correlation functions for GFP and synapsin is shown for the dendrite in (B). The shaded area indicates the results of 100 cross-correlations computed on randomized versions of the data. The upper and lower bounds of the shaded area define the 95% confidence interval.

(G) The cross-correlation functions for GFP and Y10B is shown for the dendrite in (C). The shaded area indicates the results of 100 cross-correlations computed on randomized versions of the data. The upper and lower bounds of the shaded area define the 95% confidence interval.

synthesis in hippocampal CA1 pyramidal cell dendrites via a muscarinic, NMDA-dependent mechanism. J. Neurosci. *13*, 1010–1021.

Frey, U., Krug, M., Reymann, K.G., and Matthies, H. (1988). Anisomycin, an inhibitor of protein synthesis, blocks late phases of LTP phenomena in the hippocampal CA region in vitro. Brain Res. *452*, 57–65.

Huber, K.M., Kayser, M.S., and Bear, M.F. (2000). Role for rapid dendritic protein synthesis in hippocampal mGluR-dependent long-term depression. Science *288*, 1254–1256.

Kacharmina, J.E., Job, C., Crino, P., and Eberwine, J. (2000). Stimulation of glutamate receptor protein synthesis and membrane insertion within isolated neuronal dendrites. Proc. Natl. Acad. Sci. USA *97*, 11545–11550.

Kang, H., and Schuman, E.M. (1996). A requirement for local protein synthesis in neurotrophin-induced synaptic plasticity. Science *273*, 1402–1406.

Kang, H., Shelton, D., Welcher, A., and Schuman, E.M. (1997). Neurotrophins and time: different roles for TrkB signaling in hippocampal long-term potentiation. Neuron *19*, 653–664.

Koenig, E., Martin, R., Titmus, M., and Sotelo-Silveira, J.R. (2000). Cryptic peripheral ribosomal domains distributed intermittently along mammalian myelinated axons. J. Neurosci. *20*, 8390–8400.

Lerner, E.A., Lerner, M.R., Janeway, C.A., and Steitz, J.A. (1981). Monoclonal antibodies to nucleic acid-containing cellular constituents: probes for molecular biology and autoimmune disease. Proc. Natl. Acad. Sci. USA *78*, 2737–2741.

Levine, E.S., Dreyfus, C.F., Black, I.B., and Plummer, M.R. (1995). Brain-derived neurotrophic factor rapidly enhances synaptic transmission in hippocampal neurons via postsynaptic tyrosine kinase receptors. Proc. Natl. Acad. Sci. USA *92*, 8074–8078.

Levine, E.S., Crozier, R.A., Black, I.B., and Plummer, M.R. (1997). Brain-derived neurotrophic factor modulates hippocampal synaptic transmission by increasing N-methyl-D-aspartic acid receptor activity. Proc. Natl. Acad. Sci. USA *95*, 10235–10239.

Li, Y.X., Zhang, Y., Lester, H.A., Schuman, E.M., and Davidson, N. (1998a). Enhancement of excitatory neurotransmitter release induced by BDNF in cultured hippocampal neurons. J. Neurosci. *18*, 10231–10240.

Li, Y.X., Xu, Y., Ju, D., Lester, H.A., Davidson, N., and Schuman, E.M. (1998b). Expression of a dominant negative Trk B receptor, T1, reveals a requirement for presynaptic signaling in BDNF-induced synaptic potentiation in cultured hippocampal neurons. Proc. Natl. Acad. Sci. USA *95*, 10884–10889.

Malgaroli, A., and Tsien, R.W. (1992). Glutamate-induced long-term potentiation of the frequency of miniature synaptic currents in cultured hippocampal neurons. Nature *357*, 134–139.

Martin, K.C., Casadio, A., Zhu, H., E, Y., Rose, J.C., Chen, M., Bailey, C.H., and Kandel, E.R. (1997). Synapse-specific, long-term facilitation of Aplysia sensory to motor synapses: a function for local protein synthesis in memory storage. Cell *91*, 927–938.

Mayford, M., Baranes, D., Podsypanina, K., and Kandel, E.R. (1996). The 3′-untranslated region of CAMKII-alpha is a cis-acting signal for the localization and translation of mRNA in dendrites. PNAS *93*, 13250–13255.

McAllister, A.K., Katz, L.C., and Lo, D.C. (1999). Neurotrophins and synaptic plasticity. Annu. Rev. Neurosci. *22*, 295–318.

Mori, Y., Imaizumi, K., Katayama, T., Yoneda, T., and Tohyama, M. (2000). Two cis-acting elements in the 3′ untranslated region of the alpha-CaMKII regulate its dendritic targeting. Nat. Neurosci. *3*, 1079–1084.

Nguyen, P.V., Abel, T., and Kandel, E.R. (1994). Requirement of a critical period of transcription for induction of a late phase of LTP. Science *265*, 1104–1107.

Otani, S., Marshall, C.J., Tate, W.P., Goddard, G.V., and Abraham, W.C. (1989). Maintenance of long-term potentiation in rat dentate gyrus requires protein synthesis but not messenger RNA synthesis immediately post-tetanization. Neuroscience *28*, 519–526.

Ouyang, Y., Kantor, D.B., Harris, K.M., Schuman, E.M., and Kennedy, M.B. (1997). Visualization of the distribution of autophosphorylated calcium/calmodulin-dependent protein kinase II after tetanic stimulation in the CA1 area of the hippocampus. J. Neurosci. *17*, 5416–5427.

Ouyang, Y., Rosenstein, A., Kreiman, G., Schuman, E.M., and Kennedy, M.B. (1999). Tetanic stimulation leads to increased accumulation of Ca(2+)/calmodulin-dependent protein kinase II via dendritic protein synthesis in hippocampal neurons. J. Neurosci. *19*, 7823–7833.

Patrick, G.N., Zukerberg, L., Nikolic, M., de la Monte, S., Dikkes, P., and Tsai, L.H. (1999). Conversion of p35 to p25 deregulates Cdk5 activity and promotes neurodegeneration. Nature *402*, 615–622.

Rao, A., and Steward, O. (1991). Evidence that protein constituents of postsynaptic membrane are locally synthesized: analysis of proteins synthesized within synaptosomes. J. Neurosci. *11*, 2881–2895.

Schuman, E.M. (1999a). mRNA trafficking and local protein synthesis at the synapse. Neuron *23*, 645–648.

Schuman, E.M. (1999b). Neurotrophin regulation of synaptic transmission. Curr. Opin. Neurobiol. *9*, 105–109.

Sheetz, A.J., Nairn, A.C., and Constantine-Paton, M. (2000). NMDA receptor-mediated control of protein synthesis at developing synapses. Nat. Neurosci. *3*, 211–216.

Srinivasan, Y., Guzikowski, A.P., Haugland, R.P., and Angelides, K.J. (1990). Distribution and lateral mobility of glycine receptors on cultured spinal cord neurons. J. Neurosci. *10*, 985–995.

Stanton, P.K., and Sarvey, J.M. (1984). Blockade of long-term potentiation in rat hippocampal CA1 region by inhibitors of protein synthesis. J. Neurosci. *4*, 3080–3084.

Steward, O. (1997). mRNA localization in neurons: a multipurpose mechanism? Neuron *18*, 9–12.

Steward, O., and Levy, W.B. (1982). Preferential localization of polyribosomes under the base of dendritic spines in granule cells of the dentate gyrus. J. Neurosci. *2*, 284–291.

Steward, O., and Schuman, E.M. (2001). Protein synthesis at synaptic sites on dendrites. Ann. Rev. Neurosci. *24*, 299–325.

Torre, E.R., and Steward, O. (1992). Demonstration of local protein synthesis within dendrites using a new cell culture system that permits the isolation of living axons and dendrites from their cell bodies. J. Neurosci. *12*, 762–772.

Torre, E.R., and Steward, O. (1996). Protein synthesis within dendrites: glycosylation of newly synthesized proteins in dendrites of hippocampal neurons in culture. J. Neurosci. *16*, 5967–5978.

Weiler, I.J., and Greenough, W.T. (1991). Potassium ion stimulation triggers protein translation in synaptoneurosomal polyribosomes. Mol. Cell. Neurosci. *2*, 305–314.

Weiler, I.J., and Greenough, W.T. (1993). Metabotropic glutamate receptors trigger postsynaptic protein synthesis. Proc. Natl. Acad. Sci. USA *90*, 7168–7171.

Wells, D.G., Richter, J.D., and Fallon, J.R. (2000). Molecular mechanisms for activity-regulated protein synthesis in the synapto-dendritic compartment. Curr. Opin. Neurobiol. *10*, 132–137.

Wey, C.L., Cone, R.A., and Edidin, M.A. (1981). Lateral diffusion of rhodopsin in photoreceptor cells measured by fluorescence photobleaching and recovery. Biophys. J. *33*, 225–232.

Wu, L., Wells, D., Tay, J., Mendis, D., Abbott, M.-A., Barnitt, A., Quinlan, E., Heynen, A., Fallon, J.R., and Richter, J.D. (1998). CPEB-mediated cytoplasmic polyadenylation and the regulation of experience-dependent translation of α-CAMKII mRNA at synapses. Neuron *21*, 1129–1139.

Alu sequences from GC-rich DNA are likely to be harmful and prevented from spreading in the population by natural selection. This implies no functional importance for an Alu sequence itself, but merely that, as the deletions of Alus are very unlikely to be precise, a deletion event removing an Alu is also likely to remove valuable sequences around it, and the chromosome bearing the deletion will be lost by selection.

The explanation favoured by the authors for Alu enrichment in gene-rich regions is that of positive selection in favour of Alus in GC-rich DNA. This theory, however, cannot explain the observations. The data show that Alu sequences up to five million years old are not enriched in GC-rich regions. But in human population genetics, estimated times to common ancestry of typical genomic regions show that Alu sequences which are five million years old have already been fixed (found in all individuals) in the population. This observation is also what would be expected from neutrality and genetic drift, given the human effective population size. (Alu sequences which are truly advantageous will spread to fixation much more quickly.) Earlier human ancestors would also be expected to have had similar fixation times for Alu insertions. Yet it is only during the spread to fixation of Alu sequences that positive natural selection has any opportunity to act. Thus, an increasing abundance of Alu sequences in GC-rich DNA as they age beyond five million years cannot be the result of natural selection for positive functions of Alu insertions.

**References**

1. International Human Genome Sequencing Consortium: **Initial sequencing and analysis of the human genome.** *Nature* 2001, **409**:860-921.
2. Baltimore D: **Our genome unveiled.** *Nature* 2001, **409**:814-816.

Address: Institute of Genetics, University of Nottingham, Queens Medical Centre, Nottingham NG7 2UH, UK.
E-mail john.brookfield@nottingham.ac.uk

**Primer**

# Local protein synthesis in neurons

W. Bryan Smith, Girish Aakalu and Erin M. Schuman

The processing power of the mammalian brain is derived from the tremendous interconnectivity of its neurons. An individual neuron can have several thousand synaptic connections. While these associations yield computational power, it is the modification of these synapses that gives rise to the brain's capacity to learn, remember and even recover function after injury. Inter-connectivity and plasticity come at the price of increased complexity as small groups of synapses are strengthened and weakened independently of one another (Figure 1). When one considers that new protein synthesis is required for the long-term maintenance of these changes, the delivery of new proteins to the synapses where they are needed poses an interesting problem (Figure 1). Traditionally, it has been thought that the new proteins are synthesized in the cell body of the neuron and then shipped to where they are needed. Delivering proteins from the cell body to the modified synapses, but not the unmodified ones, is a difficult task. Recent studies suggest a simpler solution: dendrites themselves are capable of synthesizing proteins. Thus, proteins could be produced locally, at or near the synapses where they are needed. This is an elegant way to achieve the synapse specific delivery of newly synthesized proteins.

Local protein synthesis is not unique to neurons. It is one of the primary mechanisms that organisms use to determine cell fate and generate differences among cells.

**Figure 1**

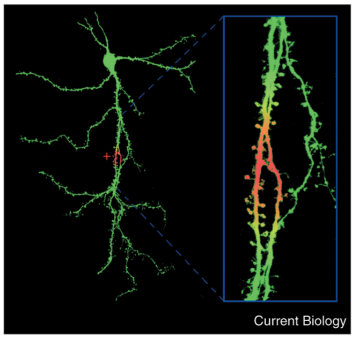


Specificity of synaptic enhancement in neurons. Shown is a single pyramidal neuron with its cell body and dendrites filled with GFP. The small protrusions that occur along the dendrites are the spines, the postsynaptic compartment onto which synapses are made. Highlighted in red is a putative area of synaptic enhancement with the adjacent yellow area depicting regions that might show a lesser amount of enhancement. During long-lasting synaptic plasticity, the spines in the enhanced area of the dendritic tree, but not the adjacent green areas, need to receive newly synthesized proteins.

For example, to achieve cellular differentiation, the *Drosophila* oocyte creates a polarized distribution of mRNA species. The mRNAs are localized and anchored to different poles of the cell *via* motifs in their 3′ untranslated regions (UTRs). The mRNAs are then locally translated to create different regions of the cell and later different daughter cells. Local protein synthesis is even used by unicellular organisms such as *Saccharomyces cerevisiae* to determine cell fate. mRNA for a factor that regulates mating type is shipped from the mother cell to the budding daughter cell, once again based on *cis*-acting elements in its 3′ UTR. The protein product restricts only the daughter cell's mating type.

Local protein synthesis is also used to create functional micro-domains within cells. Myelinating cells such as oligodendrocytes produce processes that function as

**Figure 2**

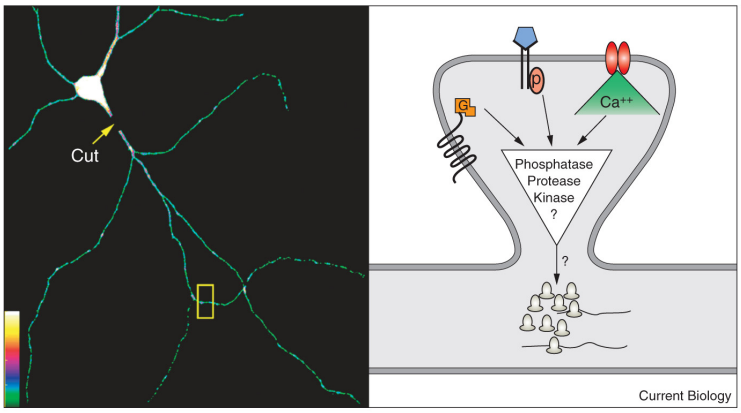


The physical isolation of dendrites from the cell body provides a definitive demonstration of local protein synthesis. Left panel: Shown is a hippocampal neuron expressing a dendritic protein synthesis reporter. A small cut isolates the cell body from the dendrites. In this cell, the application of a growth factor to the isolated dendrite resulted in dendritic protein synthesis. Right panel: Biochemical cascades that may result in protein synthesis activation. A single dendritic spine is illustrated with ribosomes at the base of the spine. Synaptic activation of metabotropic (black), growth factor (blue) and ionotropic (red) receptors may lead to dendritic protein synthesis activation through unknown intermediates.

lipid sheaths to electrically insulate axons. They do this by producing a protein called myelin basic protein that collapses the oligodendrocyte cell membrane, thus squeezing the cytoplasm out of the region where it is expressed. If myelin basic protein were produced in a cell-wide manner it would be toxic. Therefore, restricted translation of myelin basic mRNA is carried out in the oligodendrocyte processes.

Microdomains are useful not only for avoiding toxicity, but also for allowing distributed control of cellular function. Axonal growth illustrates this principle quite well. The growth cone of a developing axon must sort through a dizzying array of attractive and repulsive cues to determine how to reach the appropriate target tissue. To accomplish this task, the growth cone requires specific proteins based on environmental cues it encounters. However, the growth cone is frequently millimeters away from the soma. To solve this problem, the growth cone might locally synthesize the required proteins when it needs them. Several recent studies suggest that this is the case.

What is the evidence that distributed protein synthesis might occur during long-lasting plasticity? An early hint that local protein synthesis might occur within the dendritic compartment of neurons was the anatomical observation of synapse-associated polyribosome clusters at the base of the dendritic spine apparatus (Figure 2, right). Since those ultrastructural studies, an entire complement of translational machinery has been detected in dendrites. Additionally, several mRNA molecules are localized to the dendritic domain of neurons. Although these studies show that the components for local protein synthesis are present, they do not show that this synaptic translational machinery is actually used in response to synaptic activity.

Direct evidence supporting the local synthesis hypothesis was reported in a study by Feig and Lipton. The authors used [$^3$H]-leucine incorporation to show that new proteins were synthesized in the dendritic regions of hippocampal slice tissue following electrical stimulation. The stimulation protocol used in these studies, however, did not alter the strength of synaptic connections. In experiments using growth factor application to hippocampal slices, Kang and Schuman showed the first causal link between local protein synthesis and synaptic enhancement. In this study, brain-derived neurotrophic factor (BDNF) or neurotrophin-3 (NT-3) application to hippocampal slices was shown to elicit a long-lasting synaptic enhancement that was blocked when the tissue was pre-incubated with protein synthesis inhibitors.

In all local protein synthesis experiments, the burden of proof is to show that new proteins are made in the dendrites, not the cell body. Due to the laminar structure of the hippocampal slice, the authors were able to make microlesions that physically separated the cell bodies from the dendrites. Interestingly, even when the dendritic region was isolated, the growth factor-induced enhancement was still sensitive to protein synthesis inhibitors. Although consistent with a dendritic source of protein synthesis, this study could not distinguish between protein synthesis in dendrites, axons, glial cells or local interneurons — all of which are found within the isolated 'dendritic' laminae of hippocampal tissue.

Further evidence of activity-dependent local protein synthesis within neuronal processes has since been reported. In hippocampal slices, one form of long-term depression requires local synthesis. In the marine mollusk *Aplysia*, serotonin application results in a long-term synaptic facilitation that requires protein synthesis in the

neurites. Other studies have detected local synthesis of proteins such as calcium/calmodulin-dependent protein kinase (CamKII) following synaptic plasticity. While the data from these experiments are compelling, they lack the temporal resolution to actually watch the protein synthesis occur over time. In our recent work, we used green fluorescent protein (GFP) in combination with time-lapse microscopy to investigate local protein synthesis in dendrites of cultured hippocampal neurons. In order to rule out the cell body as a potential source of the GFP signal measured in the dendrites, we used two distinct methods of isolating the dendrites from the cell bodies. The first set of experiments employed dendritic transections, in which the dendrites were physically cut away from the cell bodies (Figure 2, left). In a less-invasive approach, the GFP in the cell body was continuously photobleached, and fluorescence was monitored in the distal dendrites. We showed that BDNF application in both experimental preparations resulted in increased GFP production in the isolated dendrites. These experiments provided the first dynamic visual proof of local protein synthesis in dendrites.

An important aspect of local protein synthesis within a micro-domain of any cell type is the transport of mRNA to the appropriate location within the cell. In the case of CamKII, *cis*-acting elements have been identified within the 3′ UTR of the mRNA molecule that are necessary and sufficient to target the message to the dendritic region of hippocampal neurons. A consensus targeting sequence has yet to be identified, but it does appear as though targeting sequences reside in the 3′ UTRs of other messages as well. Several studies show that the mRNA-binding protein Staufen, which is critically involved in mRNA localization in the *Drosophila* embryo, may also participate in mRNA trafficking to neuronal dendrites.

In addition to specific transport requirements, if a message is to have a local effect only at its destination — often a distance of several hundred microns from the nucleus — there must be control over translation of the mRNA. Without translational regulation, the protein could be produced *en route* to its destination, thereby negating any specificity that arises as a result of local synthesis. It has been recently shown that a host of mRNA binding proteins work in concert to restrict translation of certain mRNA species until the appropriate time when the protein is to be produced. Central to this process is the cytoplasmic poly-adenylation element (CPE) found in the 3′ UTR of many messages. The CPE is bound by CPE-binding protein, which forms a complex with other RNA binding proteins thus regulating translation of these messages. As the 3′ UTR sequences of more mRNAs become available, it will be interesting to discover the role the CPE and other mRNA elements play in controlling local mRNA translation.

If dendritic protein synthesis is a requirement for long-term synaptic enhancement, to what extent is activity-induced protein synthesis restricted to activated synaptic sites? In order to answer this question of synapse specificity, experiments that address the precise spatial limits of protein synthesis induction during synaptic activation must be carried out. With such information, we will begin to understand the contribution of locally synthesized synaptic proteins to the subcellular specificity of neuronal communication.

Ultimately, the upstream biochemical signaling events that lead to protein synthesis activation need to be elucidated (Figure 2, right). By understanding the transduction mechanisms that various extracellular signals use to regulate protein synthesis machinery and how differences in these signaling cascades result in translation of distinct subsets of mRNA species, a defined role for activity-dependent local translation in mature dendrites will begin to unfold.

## Key references

Aakalu G, Smith WB, Nguyen N, Jiang C, Schuman EM: **Dynamic visualization of local protein synthesis in hippocampal neurons.** *Neuron* 2001, **30:**489-502.

Bassell GJ, Zhang H, Byrd AL, Femino AM, Singer RH, Taneja KL, Lifshitz LM, Herman IM, Kosik KS: **Sorting of beta-actin mRNA and protein to neurites and growth cones in culture.** *J Neurosci* 1998, **18:**251-265.

Engert F, Bonhoeffer T: **Synapse specificity of long-term potentiation breaks down at short distances.** *Nature* 1997, **388:**279-284.

Huber KM, Kayser MS, Bear MF: **Role for rapid dendritic protein synthesis in hippocampal mGluR-dependent long-term depression.** *Science* 2000, **288:**1254-1257.

Kang H, Schuman EM: **A requirement for local protein synthesis in neurotrophin-induced hippocampal synaptic plasticity.** *Science* 1996, **273:**1402-1406.

Martin KC, Casadio A, Zhu HEY, Rose JC, Chen M, Bailey CH, Kandel ER: **Synapse-specific, long-term facilitation of aplysia sensory to motor synapses: a function for local protein synthesis in memory storage.** *Cell* 1997, **91:**927-938.

Ouyang Y, Rosenstein A, Kreiman G, Schuman EM, Kennedy MB: **Tetanic stimulation leads to increased accumulation of $Ca^{2+}$/calmodulin-dependent protein kinase II via dendritic protein synthesis in hippocampal neurons.** *J Neurosci* 1999, **19:**7823-7833.

Schuman EM, Madison DV: **Locally distributed synaptic potentiation in the hippocampus.** *Science* 1994, **263:**532-536.

Steward O, Schuman EM: **Protein synthesis at synaptic sites on dendrites.** *Annu Rev Neurosci* 2001, **24:**299-325.

Steward O, Levy WB: **Preferential localization of polyribosomes under the base of dendritic spines in granule cells of the dentate gyrus.** *J Neurosci* 1982, **2:**284-291.

Wells DG, Richter JD, Fallon JR: **Molecular mechanisms for activity-regulated protein synthesis in the synapto-dendritic compartment.** *Curr Opin Neurobiol* 2000, **10:**132-137.

Address: HHMI/Division of Biology, Caltech, Pasadena, California 91125, USA.
E-mail: schumane@its.caltech.edu

# Activation-dependent changes in receptor distribution and dendritic morphology in hippocampal neurons expressing $P2X_2$-green fluorescent protein receptors

**Baljit S. Khakh*, W. Bryan Smith, Chi-Sung Chiu, Donghong Ju, Norman Davidson, and Henry A. Lester**

Division of Biology, 156-29, California Institute of Technology, Pasadena, CA 91125

Contributed by Norman Davidson, February 21, 2001

**ATP-gated $P2X_2$ receptors are widely expressed in neurons, but the cellular effects of receptor activation are unclear. We engineered functional green fluorescent protein (GFP)-tagged $P2X_2$ receptors and expressed them in embryonic hippocampal neurons, and report an approach to determining functional and total receptor pool sizes in living cells. ATP application to dendrites caused receptor redistribution and the formation of varicose hot spots of higher $P2X_2$-GFP receptor density. Redistribution in dendrites was accompanied by an activation-dependent enhancement of the ATP-evoked current. Substate-specific mutant T18A $P2X_2$-GFP receptors showed no redistribution or activation-dependent enhancement of the ATP-evoked current. Thus fluorescent $P2X_2$-GFP receptors function normally, can be quantified, and reveal the dynamics of $P2X_2$ receptor distribution on the seconds time scale.**

ion channel | ATP | filopodia

Cationic P2X receptors mediate the "fast" milliseconds time scale actions of ATP in the nervous system (1, 2). The identity of most natively expressed P2X receptors is unclear, but many neurons express $P2X_2$ mRNA, $P2X_2$ proteins, and functional $P2X_2$-like receptors (2). For example, ATP mediates synaptic transmission in a portion of CA1 neurons (3), and postnatal hippocampal neurons express P2X receptors, which include $P2X_2$ subunits (3–7). Moreover, cytosolic ATP concentration is 1–5 mM, and ATP released during tissue damage activates neuronal P2X receptors in the periphery (1). ATP released as a synaptic transmitter and during ischemia of brain neurons may contribute to pathophysiology, but there are no available data on the cellular consequences of $P2X_2$ receptor activation or on the dynamic aspects of $P2X_2$ receptor distribution in brain neurons.

This study used $P2X_2$ receptors tagged with green fluorescent protein (GFP) in a quantitative method to study receptors expressed with recombinant Sindbis virus in embryonic hippocampal neurons. We report (*i*) the properties of functional GFP-tagged $P2X_2$ receptors, (*ii*) an optical and electrophysiological approach to measuring receptor numbers in living cells, and (*iii*) the cellular effects of P2X receptor activation.

## Materials and Methods

**Molecular Biology.** By PCR the $P2X_2$ stop codon was removed and the FLAG (f) epitope was inserted in frame with the $P2X_2$ cDNA cDNA (9). In the same PCR we inserted an *Xho*I site in the DNA. We generated GFP37 (10) with a *Xho*I site before the start codon and subcloned it into $P2X_2$-f between the *Xho*I site 3′ of the FLAG epitope and *Hin*dIII in the pcDNA3 polylinker to yield $P2X_2$-GFP. The $P2X_2$-f-GFP fragment was inserted into pSinRep5 between the *Stu*I and *Apa*I sites, and infective Sindbis particles were generated with the use of the Sindbis Expression System (http://www.invitrogen.com/). Site-directed mutagenesis was performed on the cDNAs with the use of synthetic oligonucleotides to generate K69A and T18A mutants (Quick Change; Stratagene).

**Electrophysiology and Imaging.** All cell preparations, two-electrode voltage-clamp recording of oocytes, and whole-cell patch recording of hippocampal neurons were performed by previously described methods (5, 11). Puffs (5 ms) of ATP (100 $\mu$M) were applied directly by pressure microejection to dendrites, soma, or neurites of the cell under voltage clamp (5–20 psi; 1 psi = 6.89 kPa) from 7- to 10-M$\Omega$ pipettes, with the use of a Picospritzer II (General Valve, Fairfield, NJ). We imaged hippocampal neurons with an Olympus Fluoview confocal microscope and software (http://www.olympus.com), but all analysis was performed with NIH IMAGEJ (http://rsb.info.nih.gov/ij/) and with the Fluoview software. We used an Olympus $\times$40 oil-immersion objective with a numerical aperture of 1.3. We applied test solutions to cells during imaging by switching among an array of parallel quartz tubes (320 $\mu$m i.d. and 450 $\mu$m o.d., ending $\approx$0.2 mm from the cell).

**Data Analysis.** Data were analyzed with CLAMPFIT (Axon Instruments) or ORIGIN 5.0 (Microcal Software, Northampton MA; http://www.MICROCAL.com/). Data in the text and graphs are shown as mean $\pm$ SEM from $n$ determinations as indicated. We estimated the size of the somatic compartment by applying $-5$ mV voltage jumps to neurons under voltage clamp ($-60$ mV) and with the use of the following relations: $R_s = \delta V / I_{in}$ and $C_m = \tau / R_s$, where $R_s$ is the series resistance, $\delta V$ is the change in voltage (5 mV), $I_{in}$ is the amplitude of the instantaneous current, $C_m$ is the capacitance, and $\tau$ is the time constant for the relaxation of the capacitive transient; we assumed a membrane capacitance of 0.92 pF/100 $\mu m^2$ (12). We measured the number of receptors in the somatic compartment by using the relation $I = n \cdot i \cdot p_o$, where $I$ is the peak of the macroscopic current, $i$ is the unitary current at $-60$ mV ($\approx$1 pA), $p_o$ is the open probability (0.6), and $n$ is the number of receptors open at the peak (13). For the optical determination of receptor density the measured pixel intensity was divided by 4 because the receptors are multimeric (1) and by 2 because $\approx$50% of the neuron surface is attached to the glass coverslip; the receptors here are not expected to be gated by ATP. The adjusted pixel intensity (14) was used to determine receptor numbers from standard curves (Fig. 2*F*). The coefficient of variance = SD divided by the mean for $n$ trials, where the $n$th trial is at most 20.

Abbreviations: GFP, green fluorescent protein; wt, wild type.

*To whom reprint requests should be sent at present address: Medical Research Council, Laboratory of Molecular Biology, Cambridge CB2 2QH, United Kingdom. E-mail: bsk@mrc-lmb.com.ac.uk.

The publication costs of this article were defrayed in part by page charge payment. This article must therefore be hereby marked "*advertisement*" in accordance with 18 U.S.C. §1734 solely to indicate this fact.



www.pnas.org/cgi/doi/10.1073/pnas.081089198

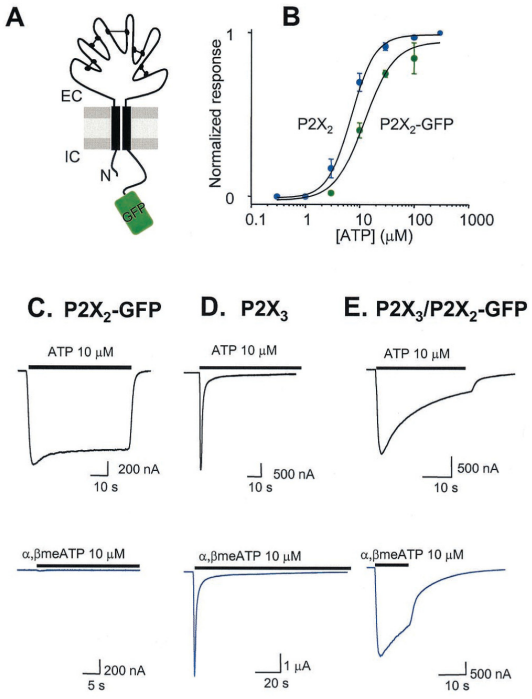


**Fig. 1.** Properties of $P2X_2$-GFP receptors. (*A*) Diagram of $P2X_2$-GFP receptor subunit topology. The folds in the extracellular loop represent hypothesized cysteine-cysteine linkages (1). (*B*) ATP concentration–effect curves for wt $P2X_2$ and $P2X_2$-GFP receptors. (*C–E*) Representative ATP and $\alpha,\beta$-methylene-ATP-evoked current waveforms from cells expressing $P2X_2$-GFP (*C*), $P2X_3$ (*D*), and $P2X_3/P2X_2$-GFP receptors (*E*). The ATP-evoked currents desensitized by 16 ± 1%, 91 ± 1% ($\tau 1 = 0.9 \pm 0.2$ s, $\tau 2 = 9 \pm 2$ s), and 63 ± 3% for $P2X_2$, $P2X_3$, and $P2X_3/P2X_2$-GFP receptors, respectively. The $\alpha,\beta$-methylene-ATP-evoked currents desensitized by 91 + 5% ($\tau 1 = 1.0 + 0.1$ s, $\tau 2 = 13 + 2$ s) and 51 + 6% for $P2X_3$ and $P2X_3/P2X_2$-GFP receptors, respectively.

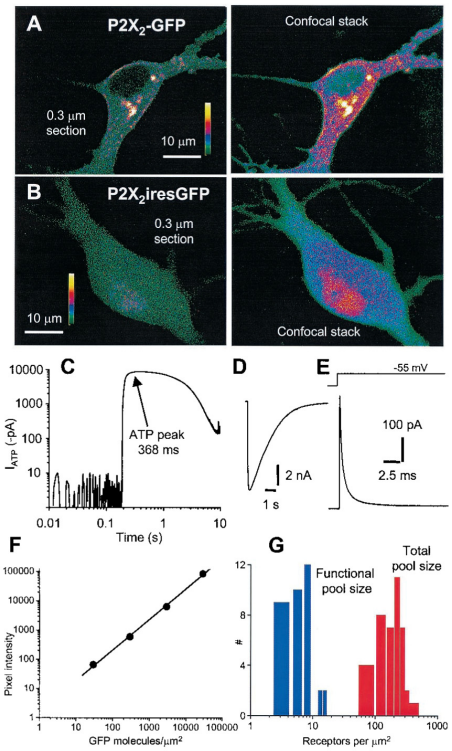


**Fig. 2.** Quantification of $P2X_2$-GFP receptors in embryonic hippocampal neurons. (*A*) (*Left*) An image through the soma of a neuron expressing $P2X_2$-GFP receptors. (*Right*) A confocal stack of 25 optical sections of the same neuron spaced at 0.3 $\mu$m. (*B*) (*Left*) An image through the soma of a neuron expressing GFP from a bicistronic $P2X_2$iresGFP mRNA. (*Right*) A confocal stack of 25 optical sections of the same neuron spaced at 0.3 $\mu$m. (*C*) Representative ATP-evoked current (100 $\mu$M, 0.5 s pulse on to soma) shown on double log scales to show that the peak was calculated at the plateau of the response at 368 ms (peak current −8.5 ± 0.5 nA, 10–90% rise time 82 ± 20 ms, 90–10% decay time 2.9 ± 0.2 s; $n = 36$). (*D*) The same current waveform as in *C*, but on linear scales. (*E*) Representative current in response to a 5 mV step from −60 mV. The trace was analyzed with the use of an equivalent circuit of the neuron somatic compartment, where $V_p$ is the pipette potential (−60 mV), $R_s$ is the series resistance (15 ± 1 MΩ), $R_m$ is the membrane resistance (741 ± 119 MΩ), $V_m$ is the membrane potential, and $C_m$ is the membrane capacitance (24.5 ± 1.6 pF; all $n = 36$). (*F*) Standard curve of GFP fluorescence intensity for agarose beads with various densities of GFP bound to the surface (14). The pixel intensity is the fluorescence intensity per pixel$^2$ of the bead surface. For high GFP densities (>100,000 GFP molecules per $\mu$m$^2$) the intensity was saturating and thus measurements were made with a neutral density filter between the objective and the charge-coupled device, and the absolute values were corrected *post hoc* (14). (*G*) Distribution of numbers of $P2X_2$ receptors per $\mu$m$^2$.

## Results

**Properties of $P2X_2$ Receptors Tagged with GFP.** We ligated GFP (10) in frame onto the C terminus of $P2X_2$ receptors (Fig. 1*A*). When expressed in *Xenopus* oocytes, $P2X_2$-GFP and wild-type (wt) receptors are similar with respect to ATP $EC_{50}$ (Fig. 1*B*) peak currents, desensitization kinetics, and suramin block {ATP $EC_{50}$ 6.5 ± 0.9 and 13.5 ± 1.5 $\mu$M, Hill slopes 1.7 ± 0.1 and 2.1 ± 0.2, for wt ($n = 8$) and $P2X_2$-GFP receptors ($n = 9$); 30 $\mu$M suramin block was 86 ± 11% and 91 ± 2%, and $k_{+1}$ was 1.2 ± 0.4 and $1.2 \pm 0.2 \times 10^4$ $M^{-1}s^{-1}$ for wt ($n = 3$) and $P2X_2$-GFP receptors ($n = 9$); where $k_{+1} = 1/\tau$[suramin]}. $P2X_2$-GFP receptors also formed a heteromer with $P2X_3$ (15), as indicated by a slowly desensitizing response to 10 $\mu$M $\alpha,\beta$-methylene-ATP, whereas $P2X_2$-GFP receptors did not respond to this agonist and $P2X_3$ receptors responded with rapidly desensitizing currents (Fig. 1 *C–E*). Thus wt and $P2X_2$-GFP receptors are similar, with the exception that $P2X_2$-GFP receptors fluoresce under blue light and thus provide a noninvasive marker for receptor location in living cells (Fig. 2).

**Density of $P2X_2$-GFP Receptors in Hippocampal Neurons.** We used Sindbis virus constructs (16) to express $P2X_2$-GFP, GFP, $P2X_2$iresGFP, T18A $P2X_2$-GFP, or K69A $P2X_2$-GFP receptors in embryonic hippocampal neurons, which are devoid of P2X receptors at this stage of development (5). Confocal laser scanning microscopy revealed that expression of $P2X_2$-GFP resulted in green fluorescence that localized to the plasma membrane and the cytosol (Fig. 2*A*), whereas expression of $P2X_2$iresGFP resulted in cytosolic green fluorescence (Fig. 2*B*). Membrane and cytosolic $P2X_2$-GFP fluorescence was notable in 0.3 $\mu$m optical sections (Fig. 2*A*), demonstrating that some $P2X_2$-GFP receptors are cytosolic, as is the case for natively expressed P2X receptors (17, 18). Capacitance measurements showed that somatic membrane area was 2449 ± 159 $\mu$m$^2$ ($n = 36$), and by measuring the peak currents evoked by a pulse of 100

$\mu$M ATP ($-8.5 \pm 0.5$ nA; $n = 36$, Fig. 2 *C* and *D*) we determined that the Sindbis vector directs the membrane expression of $6.3 \pm 0.5$ $P2X_2$-GFP receptors per $\mu m^2$ (Fig. 2 *G*; $n = 36$; see *Materials and Methods*), thus defining the somatic functional receptor pool size for these experiments.

We next exploited the fixed stoichiometry between $P2X_2$ and GFP in the fusion construct and used fluorescence microscopy to measure the somatic total $P2X_2$-GFP receptor pool size. The characterization used transparent beads with calibrated surface densities of GFP quantified with the use of an epifluorescence microscope (14) (Fig. 2*F*). We compared the fluorescence intensity of the soma with the fluorescence intensity per square micrometer of calibrated bead surface, which served as an optical standard (14). We found a value of $208 \pm 14$ receptors per $\mu m^2$ ($n = 42$) for the total somatic receptor pool size (Fig. 2*G*). Thus most $P2X_2$-GFP receptors are cytosolic, and this pool may be a source and sink for delivery to the plasma membrane.

**ATP-Induced Formation of Varicose $P2X_2$-GFP Hot Spots.** We collected images during a 1–5 min control period, then applied a pulse of either 100 $\mu$M glutamate or 100 $\mu$M ATP (10–30 s) and imaged filopodia with confocal laser scanning microscopy. We observed no change in the distribution of fluorescence with glutamate application, but during ATP application some areas increased in fluorescence; in addition, the apparent size of the fluorescent area increased within 5–10 s (Fig. 3 *A–D*). Thus ATP produced varicose hot spots (Fig. 3 *C* and *D*). The formation of varicosities was supported by similar observations in neurons infected with $P2X_2$iresGFP ($n = 8$), and this provides strong proof for a change in dendritic morphology. To quantify hot spot size we measured the intensity of pixels along a control line, during glutamate application and ATP application. Representative images of filopodia are shown in Fig. 3 *A–C*, and normalized plots for 23 line profiles are shown in Fig. 3*D*. Glutamate caused no change in the fluorescence profiles, but ATP increased the width of $P2X_2$-GFP receptor-expressing areas in regions where hot spots occur ($n = 23$). Hot spot width (at the base of the line profiles) was $1.8 \pm 0.2$ $\mu$m initially and $1.8 \pm 0.2$ $\mu$m with glutamate, but $2.9 \pm 0.3$ $\mu$m after ATP ($n = 23$). Thus the ATP-evoked hot spots in filopodia have a diameter approaching that of the varicosities, at $\approx 3$ $\mu$m.

We next chose regions of interest, *post hoc,* where hot spots formed *de novo*. We compared data on regions of interest for 86 hot spots before and during ATP application. On average there was a net increase in pixel intensity or $P2X_2$-GFP receptors in regions of interest by $66 \pm 6\%$ ($n = 86$), but pixel intensity decreased in other nearby areas within the same filopodium (Fig. 3 *E* and *F*), and there was no net increase in spatially integrated intensity (Fig. 3*E*) over entire dendritic arbors. These data imply that $P2X_2$-GFP hot spots occur because existing receptors redistribute during activation (Fig. 3).

Simple ATP-evoked depolarization is not the cause of redistribution because glutamate (100 $\mu$M) and KCl (15 mM; data not shown) did not affect $P2X_2$-GFP distribution (Fig. 3). Furthermore, we observed no ATP-evoked currents or changes in the distribution of fluorescence in neurons that expressed GFP alone or mutant K69A $P2X_2$-GFP receptors (see *Materials and Methods*; $n = 4$, Fig. 4 *A* and *C*), in which ATP binding is disrupted (19). Therefore there are no native ATP receptors that contribute to either the optical or electrophysiological responses described in this study. This observation adds credence to the analysis used to determine receptor numbers (Fig. 2 and *Materials and Methods*)

P2X receptors have at least two open states ($I_1$ and $I_2$) that differ in their permeability to organic cations. The $I_2$ state is entered in an ATP-dependent manner, has higher permeability than the $I_1$ state to some cations (5, 11, 20–22), and is absent in mutant T18A P2X receptors (23) with a disrupted protein kinase C site in the amino tail (24). In contrast to $P2X_2$-GFP receptors, mutant T18A $P2X_2$-GFP receptors did not redistribute when ATP was applied ($n = 11$, Fig. 4 *B* and *C*). T18A $P2X_2$-GFP receptors displayed rapidly desensitizing ATP-evoked responses ($n = 16$; >95% desensitization, 90–10% decay time $= 0.9 \pm 0.1$ s, and 10–90% rise time $= 59 \pm 14$ ms for a 2.5 s 100 $\mu$M ATP pulse; Fig. 4*C*), whereas $P2X_2$-GFP responses desensitized by <10% ($n = 5$; Fig. 4*C*). T18A mutant receptors are useful because they allow $P2X_2$ receptor responses to be assigned to a particular channel state, and we interpret the rapid desensitization kinetics in T18A mutants as indicative of the presence of only the $I_1$ state (23). Overall these data imply that $P2X_2$-GFP receptor redistribution and varicosity formation require prolonged $P2X_2$ receptor function, for instance, as produced by the $I_2$ state.

**Activation-Dependent Run-Up of the $P2X_2$ Current.** Our imaging experiments show that $P2X_2$-GFP receptor activation causes redistribution of fluorescence and a change in morphology, but it remained unclear whether $P2X_2$-GFP receptors move in the plasma membrane as a result of activation. To address the latter, we tested electrophysiologically for stimulation-evoked changes in functional $P2X_2$ receptors by applying ATP briefly (4–10 ms) to soma and dendrites of hippocampal neurons to approach the brevity of synaptic ATP release (25).

When ATP was puffed at a frequency of less than 0.1 Hz, the measured responses differed only slightly from puff to puff by ≤10% (the coefficient of variance was $8.9 \pm 2.2\%$ within a train of 20 responses at 0.1 Hz, and the peak of the first puff was $560 \pm 371$ pA; $n = 3$). But, remarkably, at a frequency of 1 Hz, the ATP-evoked currents increased in amplitude by $254 \pm 45\%$ from $290 \pm 64$ pA at the first puff (Fig. 5*A*; $n = 12$ of 15 neurons; three neurons showed no run-up) of the initial amplitude within 10 responses. The increase could be described by a rate constant of $\approx 0.7$ $s^{-1}$ ($1/\tau$; Fig. 5*B*). The coefficient of variance for puffs 1 through 10 was $23.5 \pm 3.5\%$ ($n = 12$), reflecting the activation-dependent run-up of the ATP-evoked current, but for trials 11 through 20 the coefficient of variance was $5.5 \pm 2.2\%$ ($n = 12$). Our measurements indicate that ≈300 $P2X_2$ receptors are activated during the first puff and, on average, that the number of functional receptors doubles within 10 repetitive puffs at 1 Hz.

Run-up was not observed when glutamate was similarly applied to hippocampal neurons ($35 \pm 13$ pA at first puff, $n = 3$; Fig. 5*B*), when ATP was applied to superior cervical ganglion neurons ($87 \pm 31$ pA at first puff, $n = 5$; Fig. 5*B*), or when ATP was applied to hippocampal neurons expressing T18A $P2X_2$-GFP mutant receptors ($1018 \pm 121$ pA at first puff; Fig. 5*B*). We also examined $P2X_3$ receptors in small-diameter dorsal root ganglion neurons; as expected, the ATP-evoked currents showed marked desensitization between trials (26) ($426 \pm 86$ pA at first puff, $n = 15$; Fig. 5*B*). Accepting the limitation that the glutamate-evoked currents were smaller than the ATP-evoked currents, we interpret these data to indicate that the ATP response in hippocampal neurons (Fig. 5*A*) was not an artifact of the puffer.

## Discussion

The present study shows that $P2X_2$ receptors tagged with GFP are functional. There were more $P2X_2$-GFP receptors in the cell than functional receptors in the membrane, and we present an electrophysiological and optical approach to measuring the number of functional receptors and the total number of receptors in living cells. We expect that similar approaches that use calibrated beads (14) as standards can be used to quantify the expression of any biologically interesting GFP-tagged proteins or organelles such as synaptic vesicles, in living cells in real time. In a previous study, $P2X_1$ receptors tagged with GFP on the C terminus were reported to internalize during ATP applications

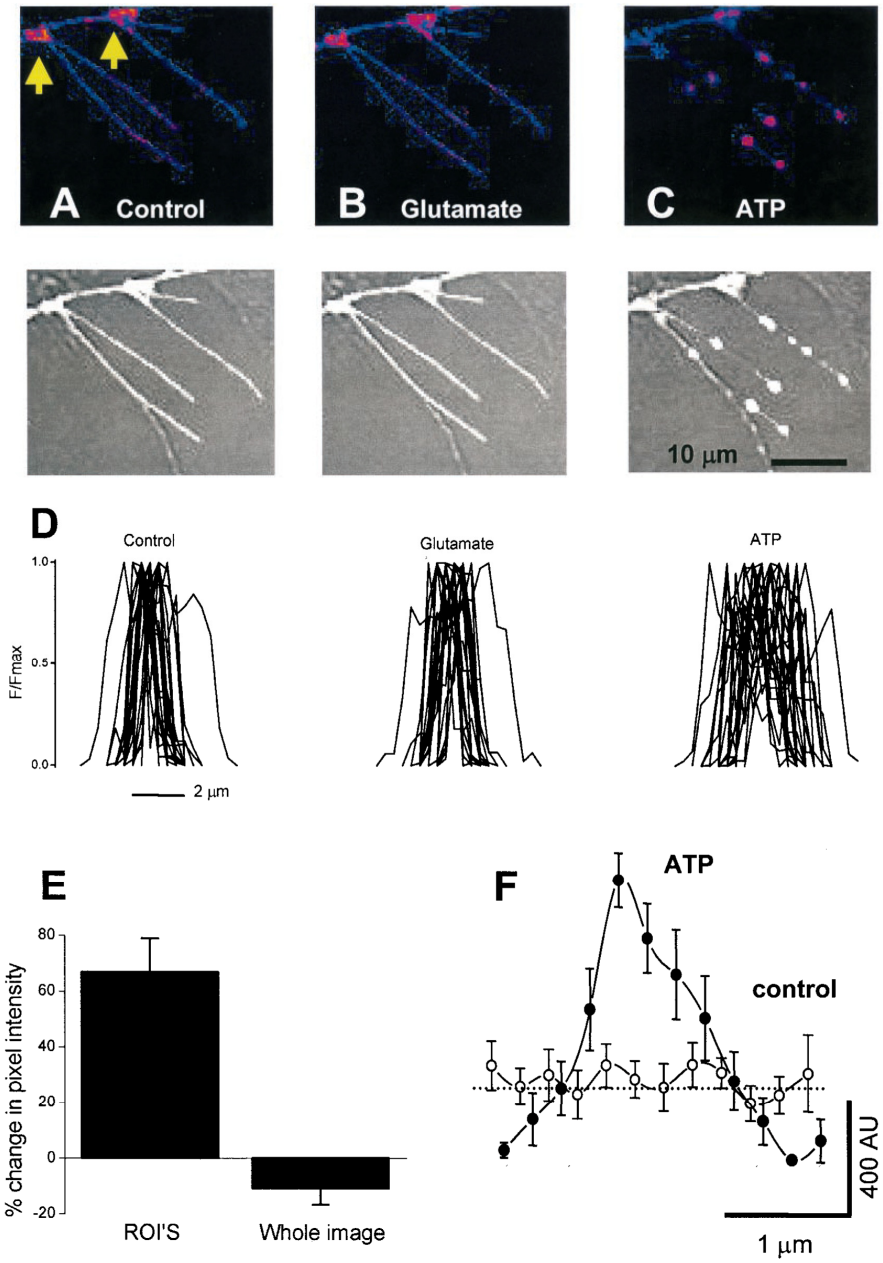


**Fig. 3.** ATP-dependent redistribution of P2X receptors in hippocampal neurons. (*A–C*) (*Upper*) False color images of filopodia from hippocampal neurons expressing $P2X_2$-GFP. (*Lower*) Overlay of gray-scale fluorescence and bright-field images. (*Left*) The control image. (*Center*) With 100 $\mu$M glutamate. (*Right*) With 100 $\mu$M ATP. (*D*) Twenty-three intensity profiles across filopodia for control, in glutamate, and in the presence of ATP. (*E*) ATP-evoked changes in integrated pixel intensity of whole dendritic arbors and regions of interest (ROI's). (*F*) Average line profile along 10 hot spots before and during ATP. AU, arbitrary units. Note the peak of the hot spot has higher fluorescence, but that $\approx$1 $\mu$m from the peak, the intensity falls to values lower than in the control.

(27). In contrast, we found no evidence for net internalization or externalization of $P2X_2$-GFP receptors expressed in hippocampal neurons when ATP was applied.

During $P2X_2$-GFP receptor activation by ATP, we observed (*i*) the formation of varicose hot spots, (*ii*) $P2X_2$-GFP redistribution over micrometer distances, and (*iii*) an activation-

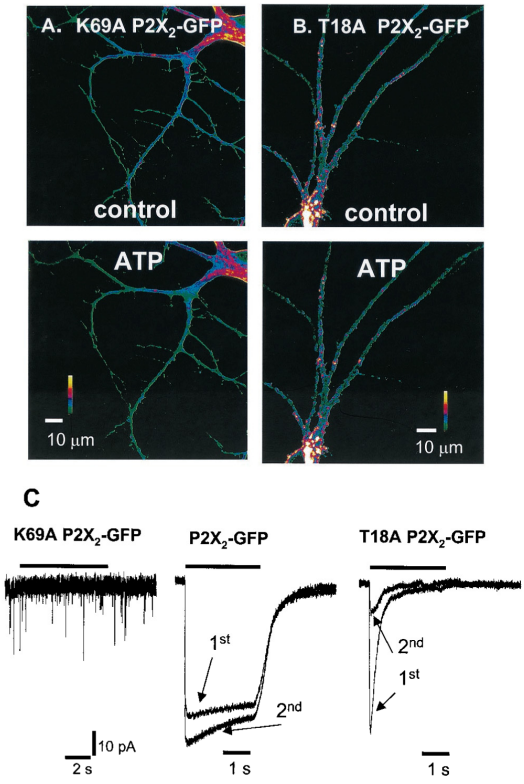


**Fig. 4.** $P2X_2$-GFP hot spots. (*A*) Representative examples of dendrites expressing K69A $P2X_2$-GFP receptors. ATP had no effect compared with the control. (*B*) Representative examples of dendrites expressing T18A $P2X_2$-GFP receptors. ATP had no effect compared with control. (*C*) (*Left*) 2.5s 100 $\mu$M ATP application did not evoke any membrane currents from this representative hippocampal neuron expressing K69A $P2X_2$-GFP receptors. The cells were healthy because glutamatergic excitatory postsynaptic currents were observed (downward deflections). (*Center*) 2.5 s 100 $\mu$M ATP-evoked currents (5 min apart) from a single hippocampal neuron expressing $P2X_2$-GFP receptors. The second response was larger than the first (see Fig. 5 for further experiments), and there was $<$10% desensitization. (*Right*) 2.5-s 100 $\mu$M ATP-evoked currents (5 min apart) from a single hippocampal neuron expressing T18A $P2X_2$-GFP receptors. Note that the second response is smaller than the first (see also Fig. 5). The traces in *Center* and *Right* are normalized to the peak of the first response.

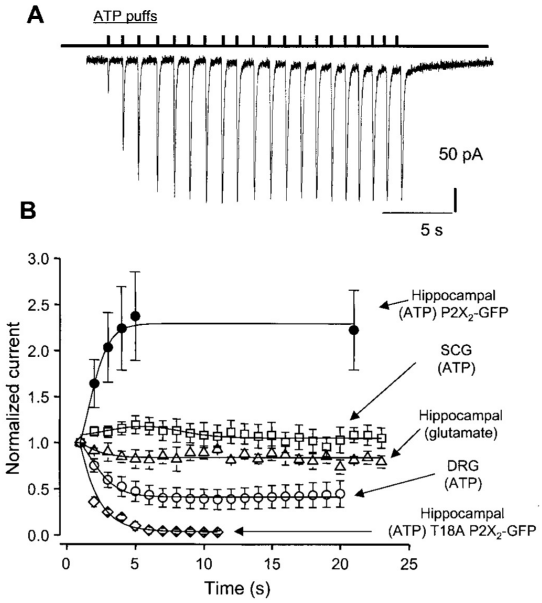


**Fig. 5.** Run-up of the P2X receptor current as a function of activation. (*A*) Representative whole-cell current recording with ATP puffed every second, for a total of 20 puffs. We could not reliably apply ATP at frequencies faster than 1 Hz. (*B*) Effect of repetitive applications of transmitter to neurons, with current normalized to the first puff. The ATP-evoked currents in hippocampal neurons increase as a function of puff number, but glutamate-evoked currents in hippocampal neurons and ATP-evoked currents in superior cervical ganglion (SCG) neurons do not. The ATP-evoked currents in dorsal root ganglion (DRG) neurons show a significant decrease in amplitude as a function of puff number, as do the ATP-evoked currents at T18A $P2X_2$-GFP receptors.

dependent enhancement of the ATP-evoked current. We detected a 66% increase in pixel intensity at the most obvious hot spots after exposure to ATP for 5–10 s. We also detected a 100% increase in ATP-evoked responses after five puffs at 1 Hz. We hypothesize that the clustering (Figs. 3*C* and 5*A*) evoked by the addition of ATP underlies the observed increase in responses to puffs of ATP. There was a difference between the electrophysiology and imaging experiments: whereas the activation-dependent current increase reversed in $\approx$10 s, the increase in pixel intensity and varicosity formation persisted for at least 5 min. Presumably, changes in dendritic morphology (varicosities) that are detected optically, but not electrophysiologically, may explain this difference. Indeed, bright-field images show a change in morphology, and a similar phenomenon was observed with $P2X_2$iresGFP, which directs the expression of cytosolic GFP.

Activation of glutamate receptors results in the formation of varicosities in neuronal processes (28), and the glutamate receptor subunit, GluR1, moves from a cytosolic pool to the plasma membrane during activity in hippocampal neurons (16). These *in vitro* studies are enlightening because glutamate-evoked morphological changes are implicated in the pathogenesis of ischemic neurotoxicity, and GluR1 redistribution may occur during synaptic plasticity (16). The present data are portentous because $P2X_2$ receptor-activation-dependent changes in neuron morphology and receptor distribution may also occur for natively expressed receptors *in vivo*. Indeed, $P2X_7$ receptor-mediated currents in microglial cells show activation-dependent increases (29), and activation of $P2X_7$ receptors evokes changes in cell morphology (30), although changes in $P2X_7$ receptor distribution were not reported. Moreover, changes in superior cervical ganglion neuron morphology occur during P2X receptor activation (11). Interestingly, $P2X_7$ receptors as well as P2X receptors in microglial cells and superior cervical ganglion neurons display the $I_2$ state. The mechanisms underlying P2X receptor-mediated changes in cell morphology are currently unknown, but our data suggest that the higher permeability $I_2$ state of $P2X_2$ receptors is required (5, 11, 20–22) and that perhaps changes previously associated with $P2X_7$ receptors (30) may also occur during activation of neuronal P2X receptors. Fluorescence redistribution and changes in ATP-evoked currents and morphology do not result in cell death because the effects were completely reversible with the brief (up to 10–30 s) applications tested in the present study. Moreover, because the T18A muta-

tion disrupts the protein kinase C consensus site of $P2X_2$ receptors (24), these data are consistent with, but do not prove, the idea that $P2X_2$ receptor properties and redistribution may be shaped by protein kinase C activity.

Native neuronal P2X receptors mediate ATP fast synaptic transmission in the peripheral, enteric, and central nervous systems and presynaptically modulate synaptic transmission (1). In the present paper we have studied $P2X_2$-GFP receptors in hippocampal neurons because these cells are known to express $P2X_2$ receptors (17) and ATP mediates a component of the excitatory postsynaptic current (3). In view of the activation-dependent nature of the redistribution, $P2X_2$ receptor-mediated excitatory postsynaptic currents may undergo short-term modulation, by a postsynaptic mechanism similar to that suggested for glutamatergic synapses (8, 16, 31, 32). Moreover, P2X receptor-mediated changes in neuron morphology may be relevant during stroke when ATP is released. Our data establish redistribution and the formation of varicosities as an interesting functional attribute of heterologously expressed neuronal $P2X_2$-GFP receptors. It remains to be determined whether these effects occur for natively expressed receptors *in vivo*, either physiologically or during disease.

We thank H. Li for preparation of *Xenopus* oocytes and E. Schuman for advice and use of the confocal microscope. This work was supported by a Wellcome Trust (U.K.) Prize Fellowship (to B.S.K.), by a Roche Bioscience Award, and by the National Institutes of Health (NS-11756, MH 49176).

1. Khakh, B. S. (2001) *Nat. Rev. Neurosci.* **2,** 165–174.
2. Khakh, B. S., Burnstock, G., Kennedy, C., King, B. F., North, R. A., Seguela, P., Voigt, M. & Humphrey, P. P. A. (2001) *Pharmacol. Rev.*, **53,** 107–118.
3. Pankratov, Y., Castro, E., Miras-Portugal, M. T. & Krishtal, O. (1998) *Eur. J. Neurosci.* **10,** 3898–3902.
4. Wong, A. Y., Burnstock, G. & Gibb, A. J. (2000) *J. Physiol. (London)* **527,** 529–547.
5. Khakh, B. S., Proctor, W. R., Dunwiddie, T. V., Labarca, C. & Lester, H. A. (1999) *J. Neurosci* **19,** 7289–7299.
6. Collo, G., North, R. A., Kawashima, E., Merlo-Pich, E., Neidhart, S., Surprenant, A. & Buell, G. (1996) *J. Neurosci.* **16,** 2495–2507.
7. Kidd, E. J., Grahames, C. B., Simon, J., Michel, A. D., Barnard, E. A. & Humphrey, P. P. (1995) *Mol. Pharmacol.* **48,** 569–573.
8. Carroll, R. C., Lissin, D. V., von Zastrow, M., Nicoll, R. A. & Malenka, R. C. (1999) *Nat. Neurosci.* **2,** 454–460.
9. Brake, A. J., Wagenbach, M. J. & Julius, D. (1994) *Nature (London)* **371,** 519–523.
10. Grabner, M., Dirksen, R. T. & Beam, K. G. (1998) *Proc. Natl. Acad. Sci. USA* **95,** 1903–1908.
11. Khakh, B., Bao, X., Labarca, C. & Lester, H. (1999) *Nat. Neurosci.* **2,** 322–330.
12. Gentet, L. J., Stuart, G. J. & Clements, J. D. (2000) *Biophys. J.* **79,** 314–320.
13. Ding, S. & Sachs, F. (1999) *J. Gen. Physiol.* **113,** 695–720.
14. Chiu, C.-S., Kartalov, E., Unger, M., Quake, S. & Lester, H. A. (2001) *J. Neurosci. Methods*, **105,** 55–63.
15. Lewis, C., Neidhart, S., Holy, C., North, R. A., Buell, G. & Surprenant, A. (1995) *Nature (London)* **377,** 432–435.
16. Shi, S. H., Hayashi, Y., Petralia, R. S., Zaman, S. H., Wenthold, R. J., Svoboda, K. & Malinow, R. (1999) *Science* **284,** 1811–1816.
17. Rubio, M. E. & Soto, F. (2001) *J. Neurosci.* **21,** 641–653.
18. Gu, B. J., Zhang, W. Y., Bendall, L. J., Chessell, I. P., Buell, G. N. & Wiley, J. S. (2000) *Am. J. Physiol.* **279,** C1189–C1197.
19. Jiang, L.-H., Rassendren, F., Surprenant, A. & North, R. A. (2000) *J. Biol. Chem.* **275,** 34190–34196.
20. Virginio, C., MacKenzie, A., Rassendren, F. A., North, R. A. & Surprenant, A. (1999) *Nat. Neurosci.* **2,** 315–321.
21. Khakh, B. S. & Lester, H. A. (1999) *Neuron* **23,** 653–658.
22. Surprenant, A., Schneider, D. A., Wilson, H. L., Galligan, J. J. & North, R. A. (2000) *J. Auton. Nerv. Syst.* **81,** 249–263.
23. Khakh, B. S., Zhou, X., Sydes, J., Galligan, J. J. & Lester, H. A. (2000) *Nature (London)* **406,** 405–410.
24. Boue-Grabot, E., Archambault, V. & Seguela, P. (2000) *J. Biol. Chem.* **275,** 10190–10195.
25. Zhou, X. & Galligan, J. J. (1996) *J. Physiol. (London)* **496,** 719–729.
26. Cook, S. P., Rodland, K. D. & McCleskey, E. W. (1998) *J. Neurosci.* **18,** 9238–9244.
27. Li, G. H., Lee, E. M., Blair, D., Holding, C., Poronnik, P., Cook, D. I., Barden, J. A. & Bennett, M. R. (2000) *J. Biol. Chem.* **275,** 29107–29112.
28. Emery, D. G. & Lucas, J. H. (1995) *Brain Res.* **292,** 161–173.
29. Chessell, I. P., Michel, A. D. & Humphrey, P. P. (1997) *Br. J. Pharmacol.* **121,** 1429–1437.
30. Virginio, C., MacKenzie, A., North, R. A. & Surprenant, A. (1999) *J. Physiol. (London)* **519,** 335–346.
31. Lissin, D. V., Carroll, R. C., Nicoll, R. A., Malenka, R. C. & von Zastrow, M. (1999) *J. Neurosci.* **19,** 1263–1272.
32. Carroll, R. C., Beattie, E. C., Xia, H., Luscher, C., Altschuler, Y., Nicoll, R. A., Malenka, R. C. & von Zastrow, M. (1999) *Proc. Natl. Acad. Sci. USA* **96,** 14112–14117.